Link: https://doi.org/10.1016/j.ijmecsci.2023.108316

Heuristic molecular modelling of quasi-isotropic auxetic metamaterials under large deformations

Luis C.M. da Silva[a,*], Nicola Grillanda[b], Siro Casolo[a]

[a] *Department A.B.C., Politecnico di Milano, Piazza Leonardo da Vinci, 20133, Milan, Italy*
[b] *Department of Civil and Structural Engineering, University of Sheffield, Mappin Street, Sheffield S1 3JD, United Kingdom*

Abstract

A two-dimensional molecular model is presented for the elastic non-linear modelling and design of meta-materials. The fundamental unit-cell, based on a heuristic molecule (HM) approach, is composed of atoms that interact through centred and non-centred spring-based bonds. The kinematics formulation allows to consider large displacements and finite strains while the specific topology of the HM can be parametrized to modify the shape of the rigid atoms and the size of the bonds. The HM is frame indifferent and provides a remarkable quasi-isotropic elastic response for both deviatoric and volumetric large deformation modes. At a macro-scale, the relationship with different continuum materials is given through a standard isotropic Cauchy up to an isotropic Cosserat solid. Evidence on the interest of the model as a calculation tool is provided by studying the elastic response of standard and auxetic materials subjected to a non-homogeneous deformation field, as well as the response of auxetic foams under large deformations. Aside the numerical agreement, it is highlighted how the tailoring of the HM topology can be effective to approximate the non-linear geometric effects that occur at finer scales of auxetic foams. In perspective, we address how the exotic mechanical properties provided by the HM, together with the assumed physical-driven framework, can foster the engineering application and the design of new meta-materials.

Keywords: Heuristic molecule, auxetic metamaterials, micropolar model, isotropic elasticity, finite strain, RBSM

*Corresponding author
Email address: luiscarlos.martinsdasilva@polimi.it (Luis C.M. da Silva)

1. Introduction

Molecular theory of elasticity provides a refined and discrete description of matter through a mechanistic model. An early formulation of the constitutive relationship for elastic solid materials, based on a model made of particles interconnected with central-forces, was investigated in the seminal works of Navier, Cauchy and Poisson [1–3]. In this model ('rari-constant' [4]), fifteen constants govern the anisotropic elasticity, which reduces to a single constant in the isotropic case. The mechanistic character of this theory envisaged to give a physical interpretation to elasticity, yet a central-force assumption is inconsistent with the Poisson's coefficient of many materials [3]. Differently, in the frame of a solid continuum approach, Green proposed an energy theory capable to overcome this limitation and the continuum models supported the great success of the finite element method in computational mechanics. Nonetheless, the limitation of the central-force scheme was overcome by Voigt and Poincarè. Voigt [5, 6] described crystals as an assemblage of structured units ('molecules') that interact in pairs through forces and couples. On the other hand, Poincaré assumed matter as particles whose interaction potential depends on the position of all body particles, the so-called 'multi-body potential' theory. Current discrete models can be ascribed into these mechanistic perspectives, such as truss or beam lattice models [7–13], rigid-bodies-spring models (RBSM) [14–17], discrete element models [18, 19], and bond-based [20–24] or state-based [25, 26] peridynamics.

Molecular models are also applied to study the mechanics of meta-materials, which are designed to reach non-standard mechanical properties at a macro-scale [27]. Experimental works [28–31] demonstrated how the internal structure topology of materials underpins some exotic features as the auxetic behaviour. Auxetic materials have a negative Poisson's ratio and yield interesting mechanical properties, such as extreme low density and softness, fracture toughness, variable porosity and permeability, among others [32]. This characteristic is retrieved by the complex kinematics that occurs at a material elementary level [28]. In the literature, several micro-structures have been investigated [33], such as re-entrant shapes [34–36], rotating rigid and semi-rigid polygons [37], crystals [38, 39], chiral structures [40, 41], truss or beam-based lattices [7–9, 11], and foams [29]. These studies are fundamental since allow to understand the importance of including both shape and orientation when modelling

the material at finer scales, but also the need of incorporating the rotational degree of freedom and the effect of geometric non-linearities.

In this study, a heuristic molecule (HM) approach is presented for the study of auxetic meta-materials. The HM considers both centred and non-centred interatomic bonds, as given in [42], and non-linear geometric (finite strain) effects. The use of force and couple interactions bypasses the rari-constant limitation about the Poisson's ratio. The specific HM topology is parametrized to extend the analysis to particles with different shape, in converse to the molecular approaches that rely on unshaped 'atoms' (particles) [43]. The assumption of shaped atoms offers physical design significance and thus the mechanical peculiarity of the HM, such as the auxetic property, can be calibrated according to the potential interest of different engineering applications. Additionally, the isotropy of the HM will be also investigated within a context of large strains.

The main objectives are twofold. Firstly, we ascertain the strain energy density equivalence between an elastic solid body modelled according to a continuum or discrete (HM) theory [4], which was proved suitable for the study of new complex materials [44]. It is demonstrated that the macro-scale mechanical analysis of materials can be based on the HM approach without forfeiting accuracy in respect to a continuum-based FE macroscopic model. A micropolar continuum within an infinitesimal strain theory is assumed [45, 46]. Moreover, displacement, strain and stress fields can be fully accounted. The size of the HM constitutes the finer scale of analysis and, therefore, a single molecule embodies all the essence of the elastic material under study. A direct consequence is the possibility of circumventing the need of a complex phenomenological modelling and homogenization, hence avoiding the mathematical passage that conceives the physical solid structure to be a continuum assemblage of material points. It also offers the possibility to couple the HM with a discrete approach at a macro-scale, at least for the cases in which the material characteristic length is significantly lower than the dimensions of the system [47–49].

Secondly, it is aimed to demonstrate that the topology of the HM can be designed to obtain a desired mechanical response. The physical advantage of the theory is thus aligned with the possibility of applying it as a calculation tool. In specific, the HM is designed to reproduce existing complex response of auxetic materials under large deformations, such as the

case of auxetic foams. Analytical models for foams [50–58] generally affect the form of elastic strain-energy potential and become implicitly related with a constitutive standpoint. Direct numerical simulations [59, 60] or multi-scale strategies [58] are also generally pursued even if require an important computation cost since both non-linear effects and internal contacts need to be reproduced at the finer scale. Therefore, a different perspective is provided for the use of molecular models in hyperelasticity problems. On one hand, the topology parametrization of the HM is explored to produce a mechanical response that is alike with the macro-response of an auxetic foam, thence able to capture the Poisson's coefficient inversion observed in foams under large deformations [61]. The source of nonlinearity remains attributed to the topology cause rather to a constitutive cause. On the other hand, the HM approach can overcome the downscaling need of current multi-scale approaches. The simulation can be performed at a material level and thus with lower computation costs.

Finally, it is noteworthy to address that the proposed HM has a methodological attitude that follows aspects confirmed by experiments, e.g. the Hooke's law, a multi-constant material model with $C_{ijhk} \neq C_{ihjk}$ at a macro-scale, the decoupling of both volumetric and deviatoric responses [62], the positivity for the elastic modules of bonds, and the assumption of 'shaped atoms'. Such methodological attitude intends to extend the advantages of the proposed model beyond a pure numerical application. Although the HM is used to describe the mechanical response of micro-structured and auxetic solids under large deformations, an effort is made to show that it can also gather a physical importance. For instance, the concept of heuristic molecule can provide a framework to predict the mechanical properties of bespoke internal topologies for the basic-unit cell, and thence it supports the design process of metamaterials that feature non-standard properties or complex macroscopic responses.

2. Non-linear bond-based molecular model

A bond-based model is presented for two-dimensional mechanical problems. The model lies on the hypothesis that a planar media is discretized by a finite number N of atoms that can carry mass and have a specific polygonal shape, being considered rigid with respect to the other components of the system. In the reference (undeformed) configuration, atoms are placed in a periodic and structured lattice form. A local condition holds, meaning that

only adjoining atoms interact by means of bonds described by a force field potential through spring elements. The full set of centred and non-centred bonds are presented in Fig. 1. Line bonds are aligned with the direction of the bonded atoms and placed along the horizontal (type c, cyan), vertical (type c, cyan), and diagonal (type r, red) directions. Shear bonds are non-centred and orthogonal to the direction of the bonded atoms, being also included with reference to mutual shear displacements (type m, magenta) and rotations (type g, green). A set of four atoms placed in a quadrilateral disposition within the initial domain Ω is referred to be a heuristic molecule (HM) [42].

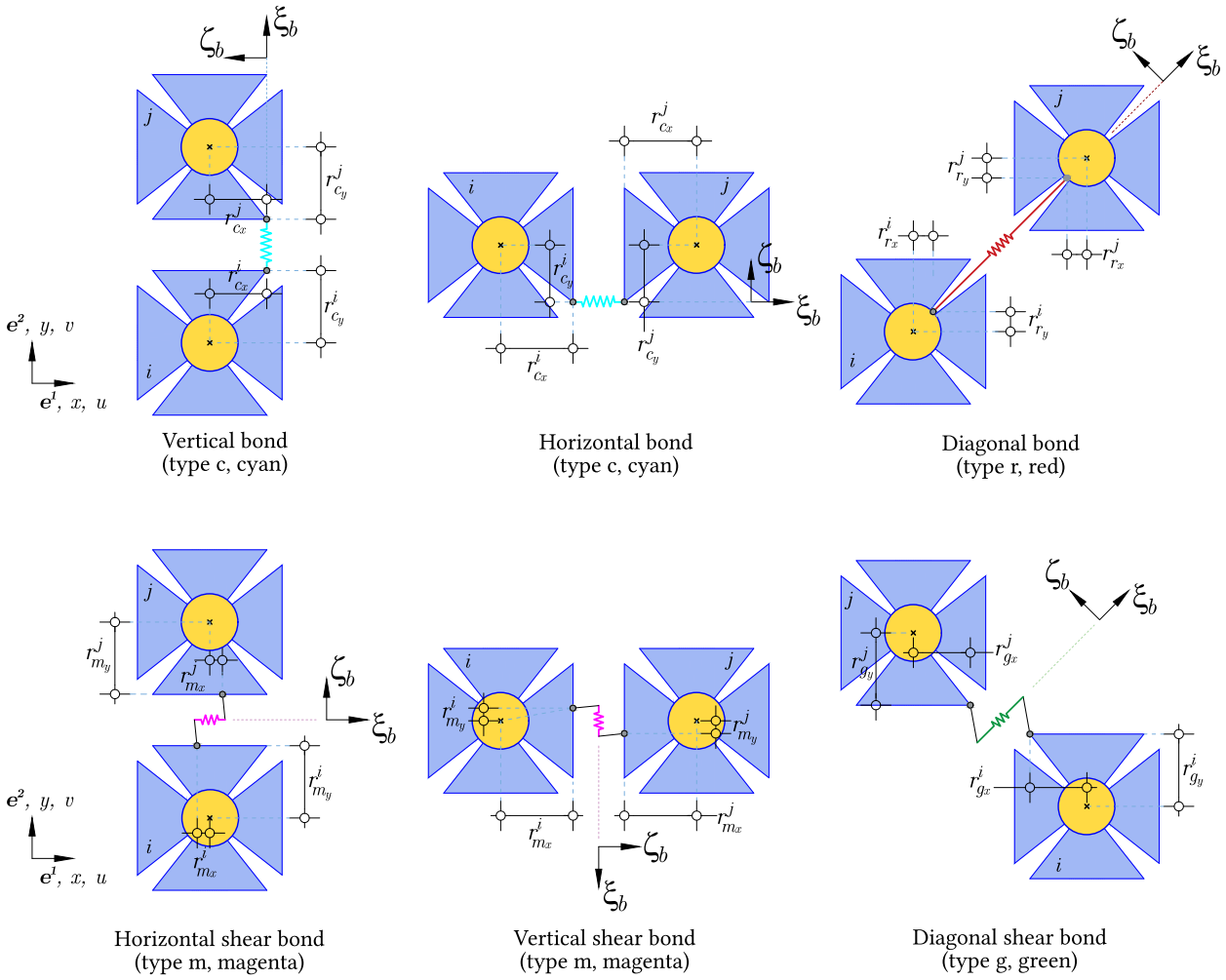

Figure 1: Conceptual scheme of the adopted two-dimensional bonds between adjoining atoms: vertical and horizontal line bonds (cyan), diagonal line bond (red), horizontal and vertical shear bond (magenta), and diagonal shear bond (green).

Considering a fixed plane Cartesian reference frame $\{O, \mathbf{e_1}, \mathbf{e_2}\}$ and a body $\mathcal{B}$ in its reference configuration, the position of the centroid of any atom i and the orientation are

given in terms of global nodal coordinates $\mathbf{x}^i = \{x^i, y^i\}^T$ in the Euclidean space $\mathcal{E}$. These positions, together with the angle ϕ^i that defines the orientation of each atoms, are gathered in the reference configuration matrices $\mathbf{X}$ and vector $\mathbf{\Phi}$, respectively:

$$\mathbf{X} = \begin{bmatrix} x^1 & x^2 & \dots & x^N \\ y^1 & y^2 & \dots & y^N \end{bmatrix}; \mathbf{\Phi} = \begin{bmatrix} \phi^1 & \phi^2 & \dots & \phi^N \end{bmatrix}, \tag{1}$$

Thus, each atom has three degrees of freedom, which correspond to two translations $\{u^i, v^i\}^T$ and one rotation ψ^i. Here, the Lagrangian coordinates are given for the N atoms as:

$$\mathbf{U} = \begin{bmatrix} u^1 & u^2 & \dots & u^N \\ v^1 & v^2 & \dots & v^N \end{bmatrix}; \mathbf{\Psi} = \begin{bmatrix} \psi^1 & \psi^2 & \dots & \psi^N \end{bmatrix}, \tag{2}$$

Accordingly, each atom i can be subjected to external nodal forces $\{p^i, q^i\}^T$ and force couple m^i, being the load matrix $\mathbf{P}$ written as:

$$\mathbf{P} = \begin{bmatrix} p^1 & p^2 & \dots & p^N \\ q^1 & q^2 & \dots & q^N \\ m^1 & m^2 & \dots & m^N \end{bmatrix} \tag{3}$$

2.1. Non-linear kinematics

The kinematic mapping χ relates the reference configuration $\mathbf{X}$ with the deformed one $\overset{\star}{\mathbf{X}}$, such that $\chi : \mathbf{X} \to \overset{\star}{\mathbf{X}}$. Fig. 2 depicts the latter relation, in which the relative Lagrangian displacements and rotations are given as $\mathbf{U} = \overset{\star}{\mathbf{X}} - \mathbf{X}$ and $\mathbf{\Psi} = \overset{\star}{\mathbf{\Phi}} - \mathbf{\Phi}$, respectively. Thence, for an arbitrary bond b within Ω that links atoms i and j, the bond vector $\mathbf{d}_b$ is given as:

$$\mathbf{d}_b = (\mathbf{x}^j + \mathbf{r}_b^j) - (\mathbf{x}^i + \mathbf{r}_b^i) \tag{4}$$

in which $\mathbf{r}_b^i$ and $\mathbf{r}_b^j$ assemble the rigid arms for the bond b in respect to atom i and j, respectively, as it was described in Fig. 1. Therefore, $\mathbf{r}_b = \mathbf{0}$ for a centred bond b.

The deformed bond vector $\overset{\star}{\mathbf{d}}_b$ that gives the direction and length of the deformed bond

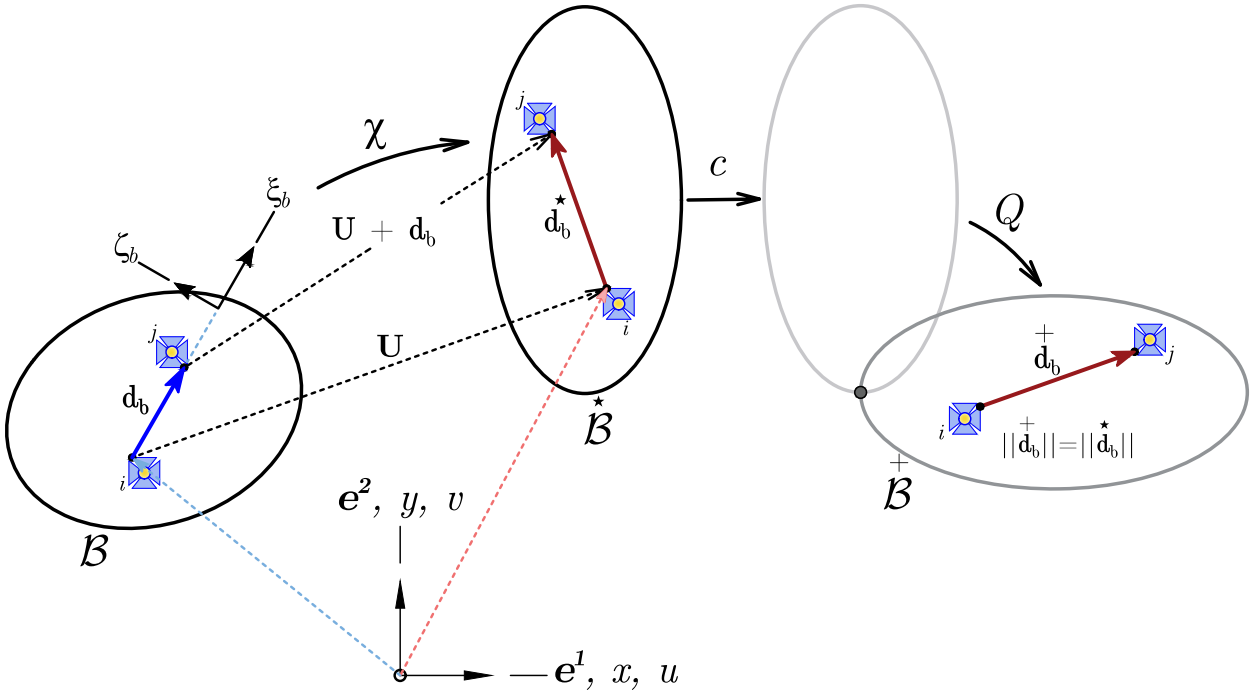

Figure 2: Relation between reference $\mathcal{B}$, elastic $\overset{\star}{\mathcal{B}}$, and transformed $\overset{+}{\mathcal{B}}$ (Euclidean transformation) configurations.

is written as:

$$\overset{\star}{\mathbf{d}}_b = (\overset{\star}{\mathbf{x}}^j + \overset{\star}{\mathbf{r}}_b^j) - (\overset{\star}{\mathbf{x}}^i + \overset{\star}{\mathbf{r}}_b^i) \tag{5}$$

in which $\overset{\star}{\mathbf{r}}_b^i$ and $\overset{\star}{\mathbf{r}}_b^j$ are the vectors that contain the rigid arms for the bond b in respect to the deformed atoms i and j, respectively. Considering atom i, the rigid arm in the deformed configuration is given as $\overset{\star}{\mathbf{r}}_b^i = (\mathbf{R}^i)^T \mathbf{r}_b^i$, in which $\mathbf{R}^i$ is a transformation matrix in respect to the global Cartesian frame:

$$\mathbf{R}^i = \begin{bmatrix} \cos(\psi^i) & -\sin(\psi^i) \\ \sin(\psi^i) & \cos(\psi^i) \end{bmatrix} \tag{6}$$

The relative displacement vector of the bond b that links atoms i and j is described as $\boldsymbol{\delta}_b$ and it is found according to the global reference frame through $\boldsymbol{\delta}_b = \overset{\star}{\mathbf{d}}_b - \mathbf{d}_b$. The general expression for $\boldsymbol{\delta}_b$ is found after some algebraic operations and given in Eq. (7). To this aim, the trigonometric relations were replaced with the corresponding Taylor expansions truncated in the second term, i.e. $\cos(\psi) \approx 1 - \frac{\psi^2}{2}$ and $\sin(\psi) \approx \psi - \frac{\psi^3}{6}$. The contribution of the linear

and non-linear parts were decoupled for convenience of reading.

$$\boldsymbol{\delta}_b = \mathbf{U}^{ij}\mathbf{A} + \mathbf{B}_b(\boldsymbol{\Psi}^{ij})^T + \frac{1}{2}\mathbf{C}_b((\boldsymbol{\Psi}^{ij})^T)^2 - \frac{1}{6}\mathbf{B}_b((\boldsymbol{\Psi}^{ij})^T)^3 \tag{7}$$

The translation relationship is described by $\mathbf{A}$, and matrices $\mathbf{B}_b$ and $\mathbf{C}_b$ gather information on the rigid arm terms with respect to the bond b as follows:

$$\mathbf{A} = \begin{bmatrix} -1 \\ 1 \end{bmatrix}; \mathbf{B}_b = \begin{bmatrix} -r^i_{b_y} & r^j_{b_y} \\ r^i_{b_x} & -r^j_{b_x} \end{bmatrix}; \mathbf{C}_b = \begin{bmatrix} r^i_{b_x} & -r^j_{b_x} \\ r^i_{b_y} & -r^j_{b_y} \end{bmatrix} \tag{8}$$

The displacements and rotations of the atoms i and j linked by a general bond are assembled as follows:

$$\mathbf{U}^{ij} = \begin{bmatrix} u^i & u^j \\ v^i & v^j \end{bmatrix}; \boldsymbol{\Psi}^{ij} = \begin{bmatrix} \psi^i & \psi^j \end{bmatrix} \tag{9}$$

2.2. Strain measure

The strain measure is evaluated at each bond and computed through the stretch ratio parameter λ that is found by considering the relative displacement vector. Thus, recalling the bond b between atom i and j, we can write:

$$\lambda_b = \frac{\|\overset{\star}{\mathbf{d}}_b\|}{\|\mathbf{d}_b\|} \tag{10}$$

The linearized strain is obtained from the variation of displacement that occurs with respect to the reference configuration. Therefore, only the component of the displacement variation projected in the local basis of the bond along the reference axis $\boldsymbol{\xi}_b$ is accounted (see Fig. 2):

$$\lambda_{b_\xi} = \frac{|\boldsymbol{\xi}_b \cdot \overset{\star}{\mathbf{d}}_b|}{\|\mathbf{d}_b\|} \tag{11}$$

The one dimensional spring-bonds allow writing the strain measure in terms of λ_b, i.e. $\epsilon_b = f(\lambda_b)$, $\epsilon_b \in \mathbb{R}$. This is convenient as the function f can be approximated by a Taylor series:

$$\epsilon_b = f(\lambda_b) + \frac{df}{d\lambda}(\lambda_b - 1) + \frac{1}{2!}\frac{d^2f}{d\lambda^2}(\lambda_b - 1)^2 + \cdots + \frac{1}{n!}\frac{d^nf}{d\lambda^n}(\lambda_b - 1)^n \tag{12}$$

In specific, and assuming that the bond has a null strain in the reference configuration, the nominal (or Engineering) strain of the bond b may be evaluated considering:

$$f = \lambda_b - 1 \tag{13}$$

and the Green-Lagrangian strain as:

$$f = \frac{1}{2}(\lambda_b^2 - 1) \tag{14}$$

Herein, we have adopted the convention that a positive and negative λ value leads to a tensile and compression strain, respectively.

2.3. Frame indifference

Considering the initial Cartesian coordinate system as reference frame for the body $\mathcal{B}$, an Euclidean transformation that preserves the length of each bond is applied to the deformed configuration $\overset{\star}{\mathcal{B}}$ and the transformed body is indicated as $\overset{+}{\mathcal{B}}$ (as depicted in Fig. 2). The single bond b, still linking atoms i and j for consistency of notation, is used herein to prove the objectivity of the constitutive equations of the presented molecular model for any Euclidean transformation. The link between the transformed $\overset{+}{\mathcal{B}}$ and deformed $\overset{\star}{\mathcal{B}}$ configurations can be written for the atom i according to Eq. (15):

$$\overset{+}{\mathbf{x}}^i + \overset{+}{\mathbf{r}}_b^i = \mathbf{c} + \mathbf{Q}(\overset{\star}{\mathbf{x}}^i + \overset{\star}{\mathbf{r}}_b^i) \tag{15}$$

in which $\overset{+}{\mathbf{x}}^i$ and $\overset{+}{\mathbf{r}}_b^i$ are, respectively, the coordinates of the atom i and the vector with the associated rigid arms after the Euclidean transformation. The latter mapping is composed by a translation $\mathbf{c}$ and rotation $\mathbf{Q}$. The transformed bond vector reads as $\overset{+}{\mathbf{d}}_b = \overset{+}{\mathbf{x}}^j + \overset{+}{\mathbf{r}}_b^j - \overset{+}{\mathbf{x}}^i - \overset{+}{\mathbf{r}}_b^i$ and, from Eq. (15), can be written as:

$$\overset{+}{\mathbf{d}}_b = (\overset{+}{\mathbf{x}}^i + \overset{+}{\mathbf{r}}_b^i - \mathbf{Q}\overset{\star}{\mathbf{x}}^i - \mathbf{Q}\overset{\star}{\mathbf{r}}_b^i) + \mathbf{Q}\overset{\star}{\mathbf{x}}^j + \mathbf{Q}\overset{\star}{\mathbf{r}}_b^j - \overset{+}{\mathbf{x}}^i - \overset{+}{\mathbf{r}}_b^i \tag{16}$$

and by rearranging the terms,

$$\overset{+}{\mathbf{d}}_b = \mathbf{Q}(\overset{\star}{\mathbf{x}}^j + \overset{\star}{\mathbf{r}}_b^j - \overset{\star}{\mathbf{x}}^i - \overset{\star}{\mathbf{r}}_b^i) = \mathbf{Q}\overset{\star}{\mathbf{d}}_b \tag{17}$$

which, bearing the orthogonal condition of $\mathbf{Q}$, put in evidence that $\|\overset{+}{\mathbf{d}}_b\| = \|\overset{\star}{\mathbf{d}}_b\|$. Any vector written according to Eq. (17) is said to be frame indifferent. Therefore, the computation of the stretch ratio according to a linearized or non-linear form, i.e. Eq. (10) and Eq. (11) respectively, is by extension frame indifferent.

It is sufficient to verify the objectivity for a single bond since the molecular model is provided by the coupling of alike bonds that are created through Euclidean transformations. In specific, the displacement vectors of a system with M bonds are assembled in the general matrix $\mathbf{D}$, which gathers the bond vectors in the form of $\boldsymbol{D} = [\mathbf{d}_1, \mathbf{d}_2, \ldots, \mathbf{d}_M]$. Its objectivity remains such that $\overset{+}{\mathbf{D}} = \mathbf{Q}\overset{\star}{\mathbf{D}}$ and:

$$\overset{+}{\mathbf{D}}^T\overset{+}{\mathbf{D}} = \overset{\star}{\mathbf{D}}^T\mathbf{Q}^T\mathbf{Q}\overset{\star}{\mathbf{D}} = \overset{\star}{\mathbf{D}}^T\overset{\star}{\mathbf{D}} \tag{18}$$

2.4. Elastic deformation energy

The interatomic bonds undergo simple axial deformations and resemble line-springs whose strain energy has, for an arbitrary bond b, a quadratic dependence on the variation of the initial bond length $L_b = \|\mathbf{d}_b\|$:

$$\mathcal{U}_b(\mathbf{d}_b, \boldsymbol{\delta}_b) = \frac{1}{2}k_c(\|\overset{\star}{\mathbf{d}}_b\| - \|\mathbf{d}_b\|)^2 = \frac{1}{2}k_c(\|\mathbf{d}_b + \boldsymbol{\delta}_b\| - \|\mathbf{d}_b\|)^2 \tag{19}$$

in which k_b is the bond stiffness. From Eq. (7), we recall that the deformation energy is related with the Lagrangian coordinates of the atoms of the system. The present energy formulation differs from the standard linearized case, which can be represented as follows:

$$\mathcal{U}_{b_\xi}(\boldsymbol{\delta}_b) = \frac{1}{2}k_b(\boldsymbol{\xi}_b \cdot \boldsymbol{\delta}_b)^2 \tag{20}$$

Additionally, it is worth observing that in the non-linear case:

$$\mathcal{U}_b(\mathbf{d}_b, \boldsymbol{\delta}_b) \neq \mathcal{U}_b(\mathbf{d}_b, -\boldsymbol{\delta}_b) \;\; \forall \boldsymbol{\delta}_b : 0 < |\boldsymbol{\delta}_b \cdot \mathbf{d}_b| < \|\boldsymbol{\delta}_b\|\|\mathbf{d}_b\| \tag{21}$$

meaning that symmetric relative displacement vectors $\boldsymbol{\delta}_b$ lead to different energy terms, except if the bond faces purely transversal (first limit case $\boldsymbol{\delta}_b \cdot \mathbf{d}_b = 0$) or purely longitudinal relative displacements (second limit case $|\boldsymbol{\delta}_b \cdot \mathbf{d}_b| = \|\boldsymbol{\delta}_b\|\|\mathbf{d}_b\|$) in respect to its local reference system ($\boldsymbol{\xi}_b$, $\boldsymbol{\zeta}_b$). To validate Eq. (21) and through simple algebraic operations, it is observed that the energy terms $\mathcal{U}_b(\mathbf{d}_b, +\boldsymbol{\delta}_b)$ and $\mathcal{U}_b(\mathbf{d}_b, -\boldsymbol{\delta}_b)$ have different definitions in the general case:

$$\begin{aligned} \mathcal{U}_b(\mathbf{d}_b, \boldsymbol{\delta}_b) &= \frac{1}{2} k_c (2\|\mathbf{d}_b\|^2 + \|\boldsymbol{\delta}_b\|^2 + 2\boldsymbol{\delta}_b \cdot \mathbf{d}_b - 2\|\mathbf{d}_b\|\|\mathbf{d}_b + \boldsymbol{\delta}_b\|) \\ \mathcal{U}_b(\mathbf{d}_b, -\boldsymbol{\delta}_b) &= \frac{1}{2} k_c (2\|\mathbf{d}_b\|^2 + \|\boldsymbol{\delta}_b\|^2 - 2\boldsymbol{\delta}_b \cdot \mathbf{d}_b - 2\|\mathbf{d}_b\|\|\mathbf{d}_b - \boldsymbol{\delta}_b\|) \end{aligned} \tag{22}$$

A schematic representation is shown in Fig. 3, in which a centred bond is depicted for the sake of simplicity. However, Eq. (21) holds for both centred and non-centred bonds.

Another consequence of the adopted formulation appears when a relative displacement vector is orthogonal to the bond vector. In fact, a null elastic deformation energy is associated in the linearized case because a null linearized stretch ratio is found according to Eq. (11), such that:

$$\mathcal{U}_{b_\xi}(\boldsymbol{\delta}_b) = 0 \Longleftrightarrow \boldsymbol{\xi}_b \cdot \boldsymbol{\delta}_b = 0 \tag{23}$$

On the other hand, the latter condition does not hold for the non-linear case. The relative displacement vector is associated to a zero elastic energy when the bond length of the reference and deformed configurations are equal, i.e. for a unitary stretch ratio according to Eq. (10). The null elastic energy condition for the non-linear case is stated as:

$$\mathcal{U}_b(\mathbf{d}_b, \boldsymbol{\delta}_b) = 0 \Longleftrightarrow \|\mathbf{d}_b + \boldsymbol{\delta}_b\| = \|\mathbf{d}_b\| \tag{24}$$

With some algebraic operations, Eq. (24) can be developed to become:

$$\mathcal{U}_b(\mathbf{d}_b, \boldsymbol{\delta}_b) = 0 \Longleftrightarrow \|\boldsymbol{\delta}_b\|^2 + 2\boldsymbol{\delta}_b \cdot \mathbf{d}_b = 0 \tag{25}$$

From a geometrical standpoint, Eq. (25) refers to the case in which the relative displacement vector defines a rigid rotations of the bond, as can be seen in Fig. 3. Equilibrium and stability of a bond with initial length l_b are ensured if, in accordance with its local coordinate axes ($\boldsymbol{\xi}_b, \boldsymbol{\zeta}_b$), and assuming no prior loading history, the following conditions are verified:

$$F_{b_\xi} = \left.\frac{\partial \mathcal{U}_b}{\partial l_b}\right|_{l_b} = 0 \ , \ \ k_c = \left.\frac{\partial^2 \mathcal{U}_b}{\partial l_b^2}\right|_{l_b} > 0 \tag{26}$$

195 in which F_{b_ξ} is the magnitude of the forces acting in the local direction $\boldsymbol{\xi}_b$ of the bond. The total potential energy of the system is found by summing the individual contribution of the bonds.

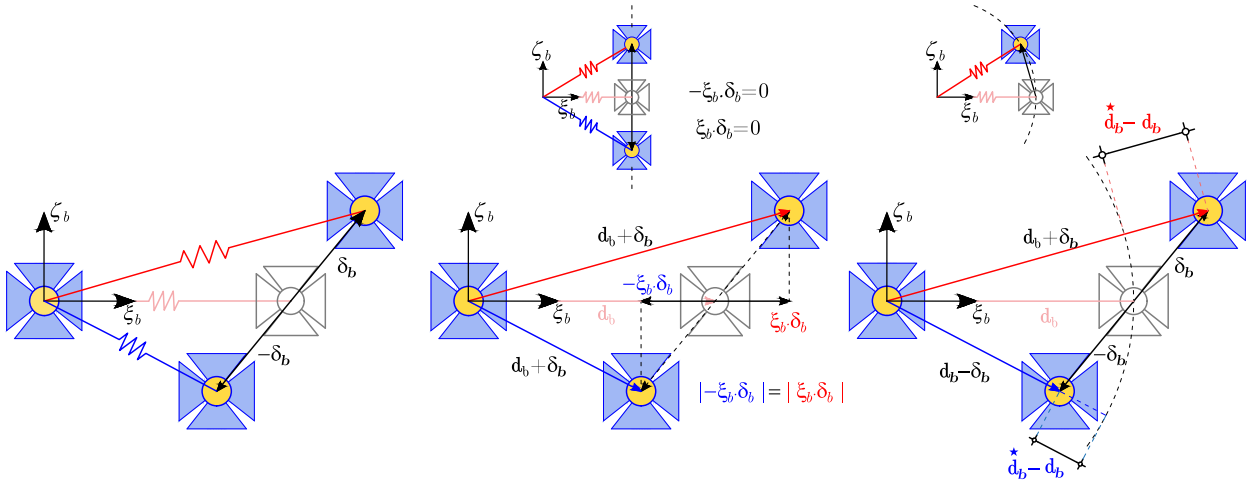

(a) Arbitrary bond b (b) Linearized theory (c) Non-linear theory

Figure 3: Single bond b subjected to (a) a symmetric relative displacements $\boldsymbol{\delta}_b$ and $-\boldsymbol{\delta}_b$. Description of the elastic deformation energies $\mathcal{U}_b$ and locus for zero-energy configurations for both (b) linearized and (c) non-linear cases.

3. Heuristic molecule

The bond-based theory of section 2 serves as basis for the proposal of a heuristic molecule 200 (HM). This section is fully dedicated to the HM since it constitutes the basic unit-cell of the theory. A framework is provided to support its application, either with a numerical purpose for the mechanical and static analysis of standard or auxetic materials, or with a practical purpose for the design of novel metamaterials.

The geometry and topology of the HM is presented first. Then, the determination of 205 strain and stress quantities within the HM is addressed. A mathematical description of the intermolecular interaction through continuum-related field quantities is convenient since a

direct interpretation of bond forces at finer scales of analysis can be difficult [63]. Nonetheless, a methodology to find the elasticity terms of bonds is also presented. It is based on an energy equivalence between a Cauchy or Cosserat [45, 64] continuum according to the hypothesis of small deformations aiming to broaden the valid range of Poisson's ratio and surpass the limitations of centred-bond theories [3]. This provides an objective approach to find the elastic stiffness of bonds according to familiar continuum-elastic parameters of materials, thence paramount for the application of the HM within a numerical study or in the design of metamaterials.

3.1. Description

The model represents two main scales of analysis. The coarser one is defined by the periodic unit-cells, which are placed in a regular way and designated as molecules. Molecules constitute the basic component of the media, beyond which the average strain and stress quantities (and stress couples) cannot be evaluated. The finer level is represented by atoms and bonds, which constitute the most fundamental components.

The molecule has been heuristically defined and is shown in Fig. 4. The interatomic distance s defines the size of the molecule. Atoms are bonded by four types of springs that can have a centred or non-centred position according to the arm vectors $\mathbf{r}_b$. Furthermore, atoms have a specific geometry, whose shape and position of bonds are given according to the HM topology that can be modified since it is parametrized. The overall size of the atom is assigned in order to exclude actions that derive from contact, thence necessarily lower than the interatomic distance s. The HM follows a structured and squared shape following the assumption that atoms are positioned in a regular lattice. These assumptions hold throughout this manuscript, and a hypothetical random arrangement of atoms is disregarded. The HM constitutes therefore the basic unit-cell of a metamaterial that is built to follow a regularly periodic internal structure. The four type of springs are here recalled in a schematic way by using their colour as reference. Each colour refers to a specific bond type. As anticipated in section 1, bonds are distinguished as: (i) horizontal and vertical axial (type c, cyan) and diagonal (type r, red) line bonds; and (ii) horizontal and vertical shear (type-m, magenta) and diagonal shear (type g, green) bonds. If a lateral separation between the horizontal and vertical bonds (type c) is accounted, then a bending moment may be reproduced and in-plane

polarity can be obtained within the molecular assemblage. In solid mechanics applications, a behaviour of this type is often associated to a heterogeneous solid with a periodic internal structure.

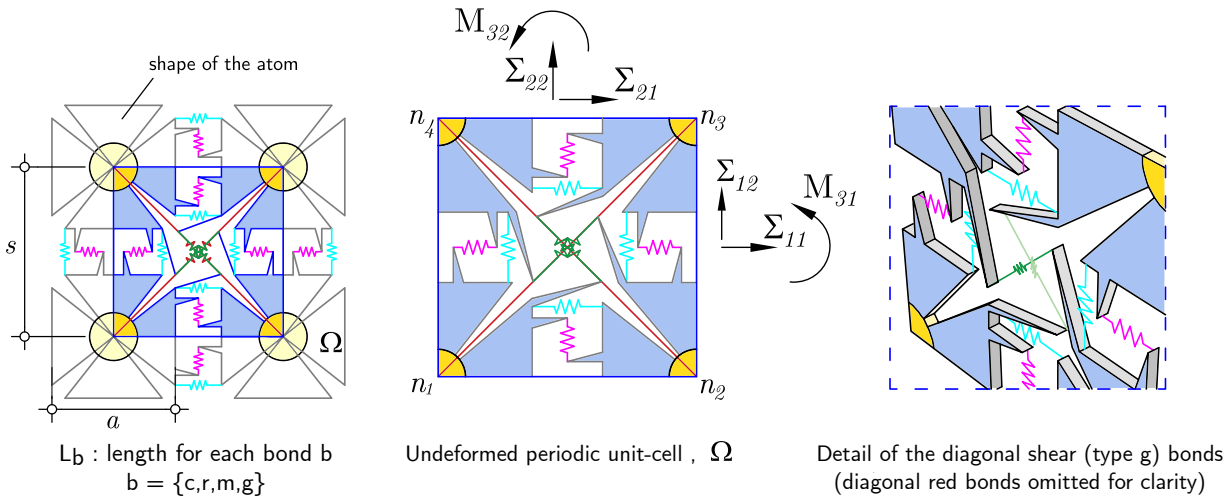

(a) Unit-cell of the Heuristic molecule (HM) in 2D and 3D

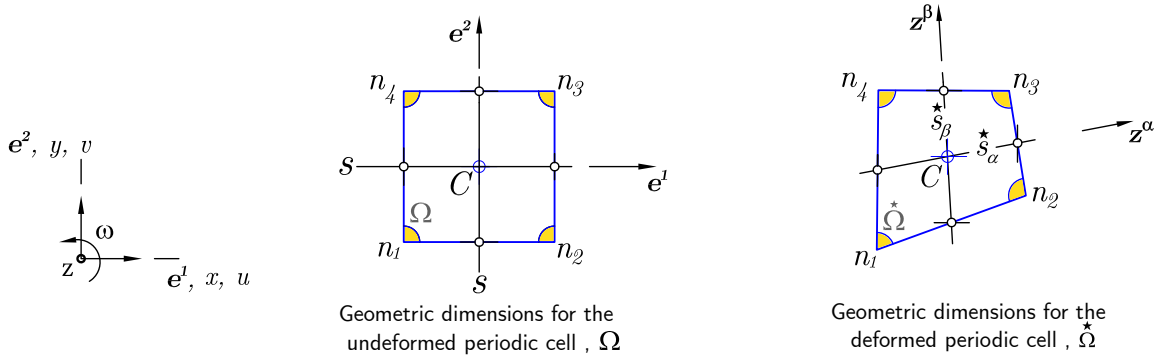

(b) Undeformed and deformed heuristic molecule

Figure 4: Topology of the adopted heuristic molecule (HM): (a) general unit-cell in the reference configuration (2D and 3D view); and (b) general dimensions for both undeformed Ω and deformed $\overset{\star}{\Omega}$ configurations.

The orientation of the more rigid subdomain of the periodic heterogeneous solid can be represented in the continuum homogenization by a unit-cell that includes an internal rotation angle. In the HM, the shear bonds (type m and g) may provide an elastic response in the presence of a micro-rotation. From a continuum standpoint, a theory with an enriched kinematics is assumed, i.e. a Cosserat continuum [45, 64] for which two displacements $\{u_1, u_2\}$ and a local rotation ω are associated to each point, whereas the internal stress is described in terms of normal, shear and micro-couple components. Therefore, for the presented model,

the equilibrium equations can be expressed by considering a non-symmetric stress tensor $S_{\alpha\beta}$ that contains normal and tangential components and a vector $M_{\alpha\beta}$ that includes the stress-couples:

$$\begin{cases} S_{\alpha\beta,\ \beta} + p_\alpha = 0 \\ M_{\alpha,\alpha} + \epsilon_{3\alpha\beta} S_{\beta\alpha} + \mu = 0 \end{cases} \quad \text{in } \Omega$$
$$\begin{cases} S_{\alpha\beta} n_\beta - s_\alpha = 0 \\ M_\alpha n_\alpha - m = 0 \end{cases} \quad \text{on } \partial\Omega \tag{27}$$

in which ϵ_{ijk} is the two-dimensional Levi-Civita tensor (or alternating symbol), ρ_α and μ represent the body forces vector and the body couple, n_α and n_β is the outward unit normal to the boundary $\partial\Omega$, and finally s_α and m are the prescribed tractions vector and couples ($\alpha, \beta = 1, 2$). The strains are conjugated in virtual work to these stress and the couple stress tensors and are given in Eq. (28) by the tensors $E_{\alpha\beta}$ and K_α, which are function of the displacements and micro-rotation.

$$\begin{aligned} E_{\alpha\beta} &= u_{\alpha\beta} + \epsilon_{3\alpha\beta}\omega_3 \\ K_\alpha &= \omega_{,\alpha} \end{aligned} \tag{28}$$

in which $\alpha, \beta = 1, 2$. From Eq. (28), it is verified that shear strains are not necessarily symmetric since are affected by the micro-rotation ω , allowing to distinguish a "symmetric shear strain" E_D , a "macro-rotation" E_ω , and a "relative micro-rotation" K_{31} (see Fig. 5) [16].

3.2. Strain and stress measures

The mathematical description of molecular interactions through continuum-related field quantities [63] is presented. A local averaging procedure to determine strain and stress measures is assumed over the basic unit-cell designated as heuristic molecule by adopting first-order homogenization concepts (Fig. 4). The displacement of a material point $\boldsymbol{x}$, the deformation gradient $\mathbf{F}$, and the displacement gradient in the reference configuration $\mathbf{H}$ are

given, respectively, by

$$\begin{aligned} \boldsymbol{u}(\boldsymbol{x}) &= \boldsymbol{\chi}(\boldsymbol{x}) - \boldsymbol{x} \\ \mathbf{F} &= \nabla \boldsymbol{\chi} \\ \mathbf{H} &= \nabla \boldsymbol{u} = \mathbf{F} - \mathbf{I} \end{aligned} \tag{29}$$

The deformation gradient $\mathbf{F}$ is a primary measure of deformation in continuum mechanics and can be related to the kinematics of the discrete model. In fact, a second-order tensor is computed for each molecule (according to Eq. (A.1) given in Appendix A) by considering the displacements of the corresponding atoms. Strain quantities can be then provided with an alike continuum mechanics form. For instance, the small-strain tensor $\boldsymbol{\varepsilon}$ and the Green-Lagrangian (finite) strain tensor $\mathbf{E}$ are given as:

$$\boldsymbol{\varepsilon} = \frac{1}{2}(\mathbf{F} + \mathbf{F}^T) - \mathbf{I} \quad ; \quad \mathbf{E} = \frac{1}{2}(\mathbf{F}^T\mathbf{F} - \mathbf{I}) \tag{30}$$

in which $\mathbf{F}^T\mathbf{F}$ represents the right Cauchy-Green deformation tensor. Accordingly, other strain measures can be obtained in agreement with continuum mechanics concepts. Before delving in the stress energy conjugates, we recall the definition of stretch ratio at a molecule level. The stretch ratios are written for each molecule according to the global coordinate system as $\lambda_1^{mol} = \frac{\overset{\star}{s}_\alpha}{s}$ and $\lambda_2^{mol} = \frac{\overset{\star}{s}_\beta}{s}$ or directly through the diagonal components of the deformation tensor, i.e. $\mathrm{diag}(\mathbf{F}) = [\lambda_1^{mol}, \lambda_2^{mol}]^T$. The convenience of stretch ratios in large deformation problems is shown in section 5.

To what concerns the stress measures, the calculation of the equivalent Cauchy-stress tensor $\boldsymbol{\Sigma}^{\boldsymbol{\sigma}}$ is introduced first through the direct estimation of the bond forces in the molecule:

$$\begin{aligned} \Sigma_{11}^{\sigma} &= \tfrac{1}{\overset{\star}{s}_\beta} \sum_b k_b \left(\overset{\star}{\boldsymbol{\xi}}_b \cdot \boldsymbol{\delta}_b\right) \left(\overset{\star}{\boldsymbol{\xi}}_b \cdot \mathbf{z}^{\boldsymbol{\alpha}}\right) \mathrm{sgn}\left(\overset{\star}{x}_j - \overset{\star}{x}_i\right) \\ \Sigma_{22}^{\sigma} &= \tfrac{1}{\overset{\star}{s}_\alpha} \sum_b k_b \left(\overset{\star}{\boldsymbol{\xi}}_b \cdot \boldsymbol{\delta}_b\right) \left(\overset{\star}{\boldsymbol{\xi}}_b \cdot \mathbf{z}^{\boldsymbol{\beta}}\right) \mathrm{sgn}\left(\overset{\star}{y}_j - \overset{\star}{y}_i\right) \\ \Sigma_{21}^{\sigma} &= \tfrac{1}{\overset{\star}{s}_\alpha} \sum_b k_b \left(\overset{\star}{\boldsymbol{\xi}}_b \cdot \boldsymbol{\delta}_b\right) \left(\overset{\star}{\boldsymbol{\xi}}_b \cdot \mathbf{z}^{\boldsymbol{\alpha}}\right) \mathrm{sgn}\left(\overset{\star}{y}_j - \overset{\star}{y}_i\right) \\ \Sigma_{12}^{\sigma} &= \tfrac{1}{\overset{\star}{s}_\beta} \sum_b k_b \left(\overset{\star}{\boldsymbol{\xi}}_b \cdot \boldsymbol{\delta}_b\right) \left(\overset{\star}{\boldsymbol{\xi}}_b \cdot \mathbf{z}^{\boldsymbol{\beta}}\right) \mathrm{sgn}\left(\overset{\star}{x}_j - \overset{\star}{x}_i\right) \end{aligned} \tag{31}$$

in which b refers to the bonds within the molecule domain Ω and independently of their nature (type c, r, m or g). The operators $\mathrm{sgn}\,(x_j - x_i)$ and $\mathrm{sgn}\,(y_j - y_i)$ provide the signal

for the difference between the coordinates of the each point i and j of the bond b in the deformed configuration:

$$\operatorname{sgn}\left(\overset{\star}{x}_j - \overset{\star}{x}_i\right) := \begin{cases} -1 & if \ \left(\overset{\star}{x}_j - \overset{\star}{x}_i\right) < 0 \\ 0 & if \ \left(\overset{\star}{x}_j - \overset{\star}{x}_i\right) = 0 \\ +1 & if \ \left(\overset{\star}{x}_j - \overset{\star}{x}_i\right) > 0 \end{cases} ; \operatorname{sgn}\left(\overset{\star}{y}_j - \overset{\star}{y}_i\right) := \begin{cases} -1 & if \ \left(\overset{\star}{y}_j - \overset{\star}{y}_i\right) < 0 \\ 0 & if \ \left(\overset{\star}{y}_j - \overset{\star}{y}_i\right) = 0 \\ +1 & if \ \left(\overset{\star}{y}_j - \overset{\star}{y}_i\right) > 0 \end{cases} \tag{32}$$

Accordingly, the first Piola Kirchhoff stress tensor (PK1) can be evaluated by considering the area vectors in the reference configuration. It is energy conjugate to the deformation gradient $\mathbf{F}$ and can be found as:

$$\begin{aligned} \Sigma_{11}^{\mathsf{PK1}} &= \tfrac{1}{s}\sum_b k_b \left(\overset{\star}{\boldsymbol{\xi}}_b \cdot \boldsymbol{\delta}_b\right)\left(\overset{\star}{\boldsymbol{\xi}}_b \cdot \mathbf{z}^{\boldsymbol{\alpha}}\right)\operatorname{sgn}\left(\overset{\star}{x}_j - \overset{\star}{x}_i\right) \\ \Sigma_{22}^{\mathsf{PK1}} &= \tfrac{1}{s}\sum_b k_c \left(\overset{\star}{\boldsymbol{\xi}}_b \cdot \boldsymbol{\delta}_b\right)\left(\overset{\star}{\boldsymbol{\xi}}_b \cdot \mathbf{z}^{\boldsymbol{\beta}}\right)\operatorname{sgn}\left(\overset{\star}{y}_j - \overset{\star}{y}_i\right) \\ \Sigma_{21}^{\mathsf{PK1}} &= \tfrac{1}{s}\sum_b k_c \left(\overset{\star}{\boldsymbol{\xi}}_b \cdot \boldsymbol{\delta}_b\right)\left(\overset{\star}{\boldsymbol{\xi}}_b \cdot \mathbf{z}^{\boldsymbol{\alpha}}\right)\operatorname{sgn}\left(\overset{\star}{y}_j - \overset{\star}{y}_i\right) \\ \Sigma_{12}^{\mathsf{PK1}} &= \tfrac{1}{s}\sum_b k_c \left(\overset{\star}{\boldsymbol{\xi}}_b \cdot \boldsymbol{\delta}_b\right)\left(\overset{\star}{\boldsymbol{\xi}}_b \cdot \mathbf{z}^{\boldsymbol{\beta}}\right)\operatorname{sgn}\left(\overset{\star}{x}_j - \overset{\star}{x}_i\right) \end{aligned} \tag{33}$$

Accordingly, the second Piola Kirchhoff stress tensor (PK2) is energy conjugate to the Green–Lagrange finite strain tensor $\mathbf{E}$ (Eq. (30)) and evaluated considering the areas and normals of the molecule planes in the reference configuration, such that:

$$\begin{aligned} \Sigma_{11}^{\mathsf{PK2}} &= \tfrac{1}{s}\sum_b k_b \left(\overset{\star}{\boldsymbol{\xi}}_b \cdot \boldsymbol{\delta}_b\right)\left(\boldsymbol{\xi}_b \cdot \mathbf{z}^{\boldsymbol{\alpha}}\right)\operatorname{sgn}\left(\overset{\star}{x}_j - \overset{\star}{x}_i\right) \\ \Sigma_{22}^{\mathsf{PK2}} &= \tfrac{1}{s}\sum_b k_b \left(\overset{\star}{\boldsymbol{\xi}}_b \cdot \boldsymbol{\delta}_b\right)\left(\boldsymbol{\xi}_b \cdot \mathbf{z}^{\boldsymbol{\beta}}\right)\operatorname{sgn}\left(\overset{\star}{y}_j - \overset{\star}{y}_i\right) \\ \Sigma_{21}^{\mathsf{PK2}} &= \tfrac{1}{s}\sum_b k_b \left(\overset{\star}{\boldsymbol{\xi}}_b \cdot \boldsymbol{\delta}_b\right)\left(\boldsymbol{\xi}_b \cdot \mathbf{z}^{\boldsymbol{\alpha}}\right)\operatorname{sgn}\left(\overset{\star}{y}_j - \overset{\star}{y}_i\right) \\ \Sigma_{12}^{\mathsf{PK2}} &= \tfrac{1}{s}\sum_b k_b \left(\overset{\star}{\boldsymbol{\xi}}_b \cdot \boldsymbol{\delta}_b\right)\left(\boldsymbol{\xi}_b \cdot \mathbf{z}^{\boldsymbol{\beta}}\right)\operatorname{sgn}\left(\overset{\star}{x}_j - \overset{\star}{x}_i\right) \end{aligned} \tag{34}$$

Moreover, expressions that resemble with classical continuum mechanics can be equivalently found. The PK1 and PK2 stress tensors can be found through the equivalent Cauchy-stress tensor $\boldsymbol{\Sigma}^{\boldsymbol{\sigma}}$ and the deformation gradient tensor $\mathbf{F}$:

$$\boldsymbol{\Sigma}^{\mathsf{PK1}} = \det(\mathbf{F})\boldsymbol{\Sigma}^{\boldsymbol{\sigma}}\mathbf{F}^{-T} \quad ; \quad \boldsymbol{\Sigma}^{\mathsf{PK2}} = \mathbf{F}^{-1}\boldsymbol{\Sigma}^{\mathsf{PK1}} \tag{35}$$

which are equivalent to Eq. (33) and Eq. (34).

3.3. Bonds stiffness

The stiffness of bonds is found by ensuring the equivalence between the discrete (molecular) and a two-dimensional continuum formulation and according to the hypothesis of small deformations. The underlying assumption is that bonds, even if dissociated from a physical representation, are used to represent the stiffness of a given material according to established deformation modes. This offers a general character to the framework since it can be applied to predict the mechanical response of any given planar system. Four deformation fields are studied to evaluate the elasticity terms of the assumed four types of spring-bonds (see Fig. 5). Three homogeneous fields given by the hydrostatic $\mathbf{H}_{\mathsf{H}}$, the deviatoric $\mathbf{H}_{\mathsf{D}}$ and the uni-axial $\mathbf{H}_{11}$ are assumed and written as:

$$\begin{aligned} \mathbf{H}_{\mathsf{H}} &= \Delta\ (\mathbf{e}^1 \otimes \mathbf{e}^1 + \mathbf{e}^2 \otimes \mathbf{e}^2) \\ \mathbf{H}_{\mathsf{D}} &= \Delta\ (\mathbf{e}^1 \otimes \mathbf{e}^2 + \mathbf{e}^2 \otimes \mathbf{e}^1) \\ \mathbf{H}_{11} &= \Delta\ (\mathbf{e}^1 \otimes \mathbf{e}^1) \end{aligned} \tag{36}$$

The fourth field is defined by a micropolar deformation $\mathbf{H}_{\omega}$ applied by imposing a micro-rotation ω to each atom. The corresponding strain energy terms of the molecule for $\mathbf{H}_{11}, \mathbf{H}_{\mathsf{H}}, \mathbf{H}_{\mathsf{D}}$ and $\mathbf{H}_{\omega}$ are given accordingly:

$$\begin{aligned} \mathcal{U}^{\mathsf{mol}}_{\mathsf{H}} &= (2c_c + c_r)\ \varepsilon^2 \quad ; \quad \mathcal{U}^{\mathsf{mol}}_{\mathsf{D}} = (c_r + 2c_m)\ \varepsilon^2 \\ \mathcal{U}^{\mathsf{mol}}_{11} &= (c_c + \tfrac{1}{4}c_r + \tfrac{1}{4}c_g)\ \varepsilon^2 \quad ; \quad \mathcal{U}^{\mathsf{mol}}_{\omega} = (c_g + 2c_m)\ \varepsilon^2 \end{aligned} \tag{37}$$

in which $\{c_c, c_r, c_m, c_g\}$ are the elastic moduli of the bonds and ε is the corresponding strain measure. These energies are written as a function of the displacement Δ to avoid the dependence of the bonds length on ε:

$$\begin{aligned} \mathcal{U}^{\mathsf{mol}}_{\mathsf{H}} &= (2k_c + 2k_r)\ (2\Delta)^2 \quad ; \quad \mathcal{U}^{\mathsf{mol}}_{\mathsf{D}} = (2k_r + 2k_m)\ (2\Delta)^2 \\ \mathcal{U}^{\mathsf{mol}}_{11} &= (k_c + \tfrac{1}{2}k_r + \tfrac{1}{2}k_g)\ (2\Delta)^2 \quad ; \quad \mathcal{U}^{\mathsf{mol}}_{\omega} = (2k_g + 2k_m)\ (2\Delta)^2 \end{aligned} \tag{38}$$

in which $\{k_c, k_r, k_m, k_g\}$ are the stiffness of the bonds. The energy terms of Eq. (38) are fundamental to find the elasticity of bonds according to different theoretical formulations, from

plane-stress to plane-strain hypotheses and either within a Classical or Cosserat continuum.

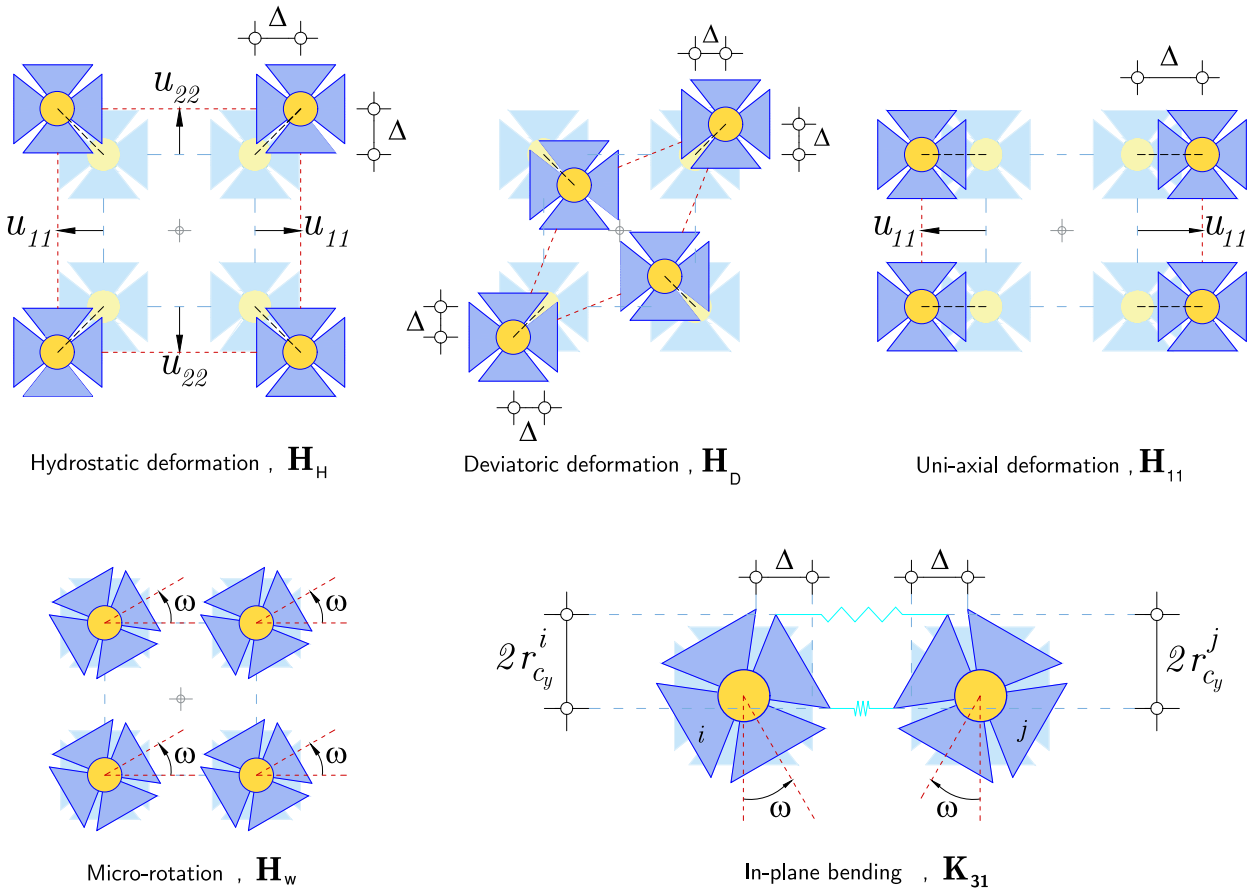

Figure 5: Homogeneous deformation fields adopted in the energy equivalence: hydrostatic $\mathbf{H}_{\mathsf{H}}$, deviatoric $\mathbf{H}_{\mathsf{D}}$, uniaxial $\mathbf{H}_{11}$, micro-rotation $\mathbf{H}_{\mathsf{W}}$ and in-plane bending $\mathbf{K}_{31}$.

3.4. Elasticity based on an isotropic Cauchy continuum

The relationship between the present heuristic molecule and the isotropic Cauchy continuum is established in terms of elastic strain energy. Given a fixed reference configuration, the deformation of the continuum solid body $\mathcal{B}$ is described by a smooth homeomorphism $\chi(\mathcal{B})$, with $\det(\nabla\chi) > 0$. The displacement of a material point $\boldsymbol{x}$, the deformation gradient $\mathbf{F}$, and the displacement gradient $\mathbf{H}$ have been already discussed. The infinitesimal strain tensor is $\boldsymbol{\varepsilon} = \mathrm{sym}\mathbf{H}$, while $\mathbf{W} = \mathrm{skw}\mathbf{H}$ characterizes the macro-rotation in the case of small $\|\mathbf{H}\|$. In the present manuscript, the case of a plane linear-elastic solid body is considered, for which:

$$\mathcal{U} = \frac{1}{2}\boldsymbol{\varepsilon}^{T}\mathbf{C}\boldsymbol{\varepsilon} \tag{39}$$

having collected the components of the infinitesimal deformation according to Voigt's notation as follows:

$$\boldsymbol{\varepsilon}^T = \left\{ E_{11}, E_{22}, E_{12}, E_{21} \right\} \tag{40}$$

while the elasticity matrices based on the hypothesis of plane-strain $\mathbf{C}^{\mathsf{PE}}$ and plane-stress $\mathbf{C}^{\mathsf{PS}}$ are, respectively, given by:

$$\mathbf{C}^{\mathsf{PE}} = 2G \begin{bmatrix} \frac{1-\nu}{1-2\nu} & \frac{\nu}{1-2\nu} & 0 & 0 \\ \frac{\nu}{1-2\nu} & \frac{1-\nu}{1-2\nu} & 0 & 0 \\ 0 & 0 & \frac{1}{2} & \frac{1}{2} \\ 0 & 0 & \frac{1}{2} & \frac{1}{2} \end{bmatrix} \quad , \quad \mathbf{C}^{\mathsf{PS}} = 2G \begin{bmatrix} \frac{1}{1-\nu} & \frac{\nu}{1-\nu} & 0 & 0 \\ \frac{\nu}{1-\nu} & \frac{1}{1-\nu} & 0 & 0 \\ 0 & 0 & \frac{1}{2} & \frac{1}{2} \\ 0 & 0 & \frac{1}{2} & \frac{1}{2} \end{bmatrix} \tag{41}$$

in which G is the shear modulus. The corresponding strain energies are determined:

$$\begin{aligned} \mathcal{U}_{11}^{\mathsf{PE}} &= \frac{G(1-\nu)}{1-2\nu}\Delta^2 \quad , \quad \mathcal{U}_{11}^{\mathsf{PS}} = \frac{G}{1-\nu}(\Delta)^2 \\ \mathcal{U}_{\mathsf{H}}^{\mathsf{PE}} &= \frac{2G}{1-2\nu}\Delta^2 \quad , \quad \mathcal{U}_{\mathsf{H}}^{\mathsf{PS}} = \frac{2G(1+\nu)}{1-\nu}\Delta^2 \\ \mathcal{U}_{\mathsf{D}}^{\mathsf{PE}} &= 2G\Delta^2 \quad , \quad \mathcal{U}_{\mathsf{D}}^{\mathsf{PS}} = 2G\Delta^2 \end{aligned} \tag{42}$$

The superscripts PE and PS refers to the plane strain and plane stress respectively, while the subscripts H, D and 11 refer to the hydrostatic, deviatoric and uniaxial homogeneous deformations. The values of the stiffness modulus assigned to the four types of bonds are obtained by comparing Eqs. (38) and (42) for $\mathbf{H}_{11}, \mathbf{H}_{\mathsf{H}}, \mathbf{H}_{\mathsf{D}}$:

$$\begin{aligned} k_c^{\mathsf{PE}} &= G \quad , \quad k_c^{\mathsf{PS}} = G \\ k_r^{\mathsf{PE}} &= 2G\tfrac{\nu}{1-2\nu} \quad , \quad k_r^{\mathsf{PS}} = 2G\tfrac{\nu}{1-\nu} \\ k_m^{\mathsf{PE}} &= G\tfrac{1-4\nu}{1-2\nu} \quad , \quad k_m^{\mathsf{PS}} = G\tfrac{1-3\nu}{1-\nu} \end{aligned} \tag{43}$$

The green spring bond has $k_g = 0$ for a Cauchy-based heuristic molecular model. The domain of application of the Cauchy-based molecule is found by respecting the equilibrium and stability conditions of Eq. (26). In specific, the latter can be guaranteed for PE and PS conditions if $(1-4\nu) \geq 0$ and $(1-3\nu) \geq 0$, respectively. This implies that the Poisson's coefficient is limited to $\nu \in [0, \frac{1}{4}]$ for PE and $\nu \in [0, \frac{1}{3}]$ for PS. It is hence noteworthy to

address that the range of application is defined by the stiffness of the bonds that govern the horizontal and shear responses (type m, magenta spring-bond).

3.5. Elasticity based on an isotropic micropolar continuum

The topology of the HM, which will be adopted for the quasi-isotropic non-linear auxetic material design, can be related to a Cosserat continuum. The constitutive response in isotropic linear-elasticity [42, 45, 64] is given by:

$$\begin{Bmatrix} \Sigma_{11} \\ \Sigma_{22} \\ \Sigma_{12} \\ \Sigma_{21} \\ M_{13} \\ M_{23} \end{Bmatrix} = \begin{bmatrix} \mathsf{C}_{1111} & \mathsf{C}_{1122} & 0 & 0 & 0 & 0 \\ \mathsf{C}_{1122} & \mathsf{C}_{2222} & 0 & 0 & 0 & 0 \\ 0 & 0 & G(1+\theta) & G(1-\theta) & 0 & 0 \\ 0 & 0 & G(1-\theta) & G(1+\theta) & 0 & 0 \\ 0 & 0 & 0 & 0 & 2Gd^2 & 0 \\ 0 & 0 & 0 & 0 & 0 & 2Gd^2 \end{bmatrix} \begin{Bmatrix} E_{11} \\ E_{22} \\ E_{12} \\ E_{21} \\ K_{13} \\ K_{23} \end{Bmatrix} \tag{44}$$

in which $\mathsf{C}_{1111}, \mathsf{C}_{2222}$ and C_{1122} are given in Eq.(41) for both PS and PE formulations; the coefficient θ governs the specific skew symmetric contribution to the shear elastic response; and d is the internal characteristic length associated to in-plane bending. For the HM and as described in Fig. 5, the quantity arms r_{c_y} and r_{c_x} define, respectively, the distances of the horizontal and vertical axial (type c, cyan) bonds to the corresponding axis of rotation of the atom. For the sake of simplicity, both arms are considered to be identical and only the module of the arm vector $\|\mathbf{r}_c\|$ is reported. The in-plane bending is governed by the non-centred type-c bonds ($\|\mathbf{r}_c\| \neq 0$), being the flexural stiffness $2Gd^2$ in Eq.(44) dependent on the component $\|\mathbf{r}_c\|$. The flexural stiffness term can be evaluated by comparing the elastic energy stored in the unit-cell with the corresponding energy stored in a Cosserat solid continuum cell subjected to an in-plane curvature $K_{31} = \frac{\omega}{s/2} = \frac{\delta}{(s/2)^2}$, such that:

$$\mathcal{U}_{\mathsf{K}}^{\mathsf{HM}} = c_c \left(\frac{2\|\mathbf{r}_c\|}{s} \right)^2 \omega^2 = Gd^2 K_{31}^2 = \mathcal{U}_{\mathsf{K}}^{\mathsf{Cosserat}} \tag{45}$$

The in-plane bending and the micropolar modes, together with the three homogeneous deformations established in Eq.(42), allow finding the stiffness terms of the bonds and the

parameter θ through the energy equivalence:

$$\begin{aligned} \mathcal{U}_{\mathsf{K}}^{\mathsf{HM}} &= \; k_c \|\mathbf{r}_c\|^2 \; \Delta^2 \qquad ; \quad \mathcal{U}_{\mathsf{K}}^{\mathsf{Cosserat,PE}} = \mathcal{U}_{\mathsf{K}}^{\mathsf{Cosserat,PS}} = G d^2 \; \Delta^2 \\ \mathcal{U}_{\omega}^{\mathsf{HM}} &= (\; 2k_g + \; 2k_m) \; \Delta^2 \quad ; \quad \mathcal{U}_{\omega}^{\mathsf{Cosserat,PE}} = \mathcal{U}_{\omega}^{\mathsf{Cosserat,PS}} = 2G\theta \; \Delta^2 \end{aligned} \tag{46}$$

Thence, for a plane-strain (PE) problem:

$$\begin{gathered} k_c^{\mathsf{PE}} = G\Big(\tfrac{d}{\|\mathbf{r}_c\|}\Big)^2 \quad ; \quad k_r^{\mathsf{PE}} = \tfrac{G}{1-2\nu} - k_c \quad ; \quad k_m^{\mathsf{PE}} = -2G\tfrac{\nu}{1-2\nu} + k_c \\ k_g^{\mathsf{PE}} = G - k_c \quad ; \quad \theta^{\mathsf{PE}} = \tfrac{1-4\nu}{1-2\nu} \end{gathered} \tag{47}$$

and for a plane-stress (PS) problem:

$$\begin{gathered} k_c^{\mathsf{PS}} = G\Big(\tfrac{d}{\|\mathbf{r}_c\|}\Big)^2 \quad , \quad k_r^{\mathsf{PS}} = G\tfrac{1+\nu}{1-\nu} - k_c \quad , \quad k_m^{\mathsf{PS}} = -2G\tfrac{\nu}{1-\nu} + k_c \quad , \\ k_g^{\mathsf{PS}} = G - k_c \quad , \quad \theta^{\mathsf{PS}} = \tfrac{1-3\nu}{1-\nu} \end{gathered} \tag{48}$$

which implies that $d = \|\mathbf{r}_c\|$, being $k_c = G$. This result also offers a practical interpretation to the geometry-based parameter d, which is equal to the arm of the cyan spring-bonds that govern the micropolar in-plane stiffness. It can be noted that the last relationship between the Poisson's ratio and the parameter θ, implies that $\mathsf{C}_{12} = \mathsf{C}_{34}$. According to Eqs. (47-48) and to guarantee that all the stiffness terms remain positive, the auxetic response is eligible only when $k_c = [0, G]$. In the case $k_c = 0$, the green bonds have the maximum stiffness and, in converse, these vanish when $k_c = G$. From these expressions, it is also worth noting that the range of Poisson's ratios that can be reproduced by the molecule is a function of k_c. The minimum and the maximum values of the Poisson's interval is determined by the magenta and the red bonds, respectively, such that:

$$k_c \in \;]0, G] \; \rightarrow \; \nu^{\mathsf{PE}} \in \left[\; \tfrac{k_c - G}{2k_c} \; , \; \tfrac{k_c}{2G + 2k_c} \; \right] \; , \; \nu^{\mathsf{PS}} \in \left[\; \tfrac{k_c - G}{k_c + G} \; , \; \tfrac{k_c}{2G + k_c} \; \right] \tag{49}$$

in which $\nu^{\mathsf{PE}} = \nu^{\mathsf{PS}} = [-1, 0]$ for the particular case $k_c = 0$, meaning that only soft auxetic materials can be reproduced or, as limit case, a soft material with null Poisson's ratio.

4. Isotropic mechanical properties of the molecule

The isotropy of the discrete model is investigated in finite strain conditions and for both plane-stress (PS) and plane-strain (PE) problems. The analytical expressions are evaluated for the linear and non-linear strain energy stored in the molecule when subjected to a given deformation $\mathbf{F}_\alpha$. Here, the subscript α represents a rotation angle with respect to the principal reference system. The rotated deformation gradient is defined as $\mathbf{F}_\alpha = \mathbf{R}_\alpha \mathbf{F} \mathbf{R}_\alpha^T$, in which $\mathbf{R}$ is the rotation matrix given in Eq. (50). The reference deformation $\mathbf{F}$ is provided by two deformation modes, i.e. the uniaxial $\mathbf{H}_{11}$ and the deviatoric $\mathbf{H}_{\mathsf{D}}$.

$$\mathbf{R} = \begin{bmatrix} \cos(\alpha) & -\sin(\alpha) \\ \sin(\alpha) & \cos(\alpha) \end{bmatrix} \tag{50}$$

The analytical expressions found for the linear and non-linear strain energies are reported in Appendix B. In the linearized case, a perfect isotropy is guaranteed if the following relation is satisfied:

$$k_c - k_r - k_m + 2k_g = 0 \tag{51}$$

This condition is dependent only on the bonds stiffness (retrieved from Eq. (47) for PE or Eq. (48) for PS case). Note that Eq. (51) is satisfied for both cases, meaning that the present heuristic molecule is fully isotropic under small displacements. Such a condition is not sufficient in the non-linear case since the strain energy is also affected by the length of bonds and by the applied deformation magnitude Δ. In this case, the isotropy is evaluated considering the variation of the ratio $\mathcal{U}(\alpha)/\mathcal{U}(0)$, in which $\mathcal{U}(\alpha)$ is the strain energy associated to a rotated deformation $\mathbf{F}_\alpha$. Results are depicted in Fig. 6 for three cases: $k_c = 0$ that leads to a ultra-soft and auxetic material; $k_c = \frac{G}{2}$ that leads to a material characterized as in-between a soft and standard response, but still able to be auxetic; and $k_c = G$ that leads to a standard material. In Fig. 6, the curves related with PE and PS are provided with blue and red lines, respectively. Furthermore, several deformations have been evaluated, being the higher differences inherently associated with the maximum deformation considered of 20%. For smaller deformations, a remarkable isotropic response is observed.

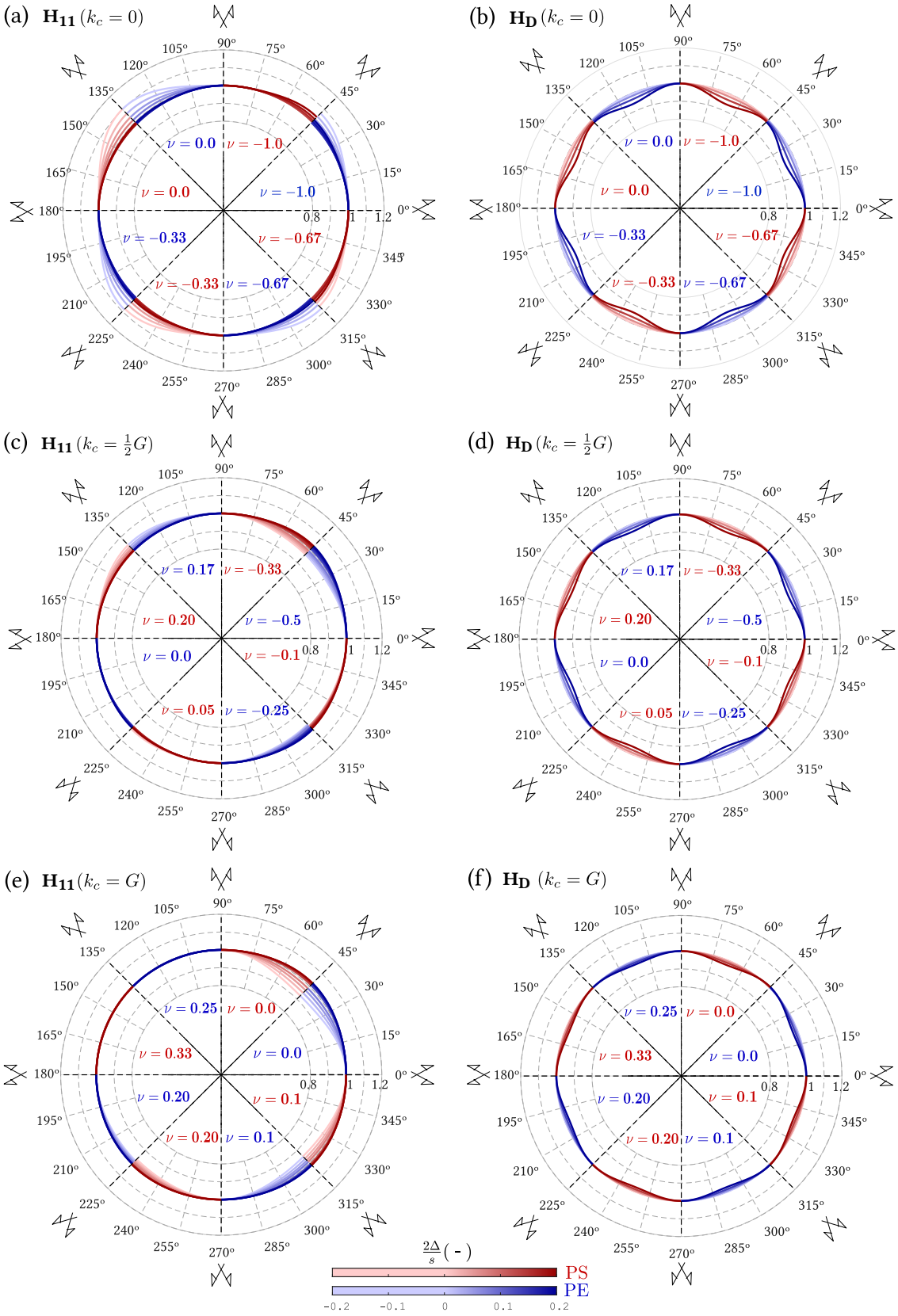

Figure 6: Elastic isotropy ratio $\mathcal{U}(\alpha)/\mathcal{U}(0)$ of the molecule for different Poisson's ratio under PS (red) and PE (blue) conditions: case $k_c = 0$ for (a) $\mathbf{H}_{11}$ and (b) $\mathbf{H}_{\mathsf{D}}$; case $k_c = \frac{1}{2}G$ for (c) $\mathbf{H}_{11}$ and (d) $\mathbf{H}_{\mathsf{D}}$; and case $k_c = G$ for (e) $\mathbf{H}_{11}$ and (f) $\mathbf{H}_{\mathsf{D}}$.

Considering the higher deformation of 20% ($|\frac{2\Delta}{s}| = 0.2$), the molecule still shows a remarkable quasi-isotropic response. The maximum difference ranges 10% for the ultra-soft auxetic molecule ($k_c = 0$) with null Poisson and under a uni-axial deformation with directions $\alpha = 45, 135, 225$ and 315 degrees (Fig. 6a). The data gathered in Fig. 6 was obtained for a HM with physically admissible lengths for bonds, i.e. $L_c = s$, $L_r = \sqrt{2}s$, $L_m = L_g = a$. However, any bond length L_b could be attributed within a problem with a mathematical purpose only. The effect that different bond lengths yield on the isotropy ratio is further investigated in Fig. 7 for both the $\mathbf{H}_{11}$ and $\mathbf{H}_{\mathsf{D}}$ deformations. The analysis is conducted for the molecule with $k_c = 0$ and $v = 0.0$. A general increase of L_b leads to lower relative errors with the reference deformation energy $\mathcal{U}(\alpha)$ and, consequently, to the improvement of the HM isotropy. Further information on the corresponding reference (linearized) and non-linear energy terms and the expressions of the partial derivatives $\frac{\partial \mathcal{U}}{\partial L_b}$ are reported in Appendix B and Appendix C. Such analysis gathers particular relevance since the size for bonds can be established beforehand to design molecules with different isotropy levels.

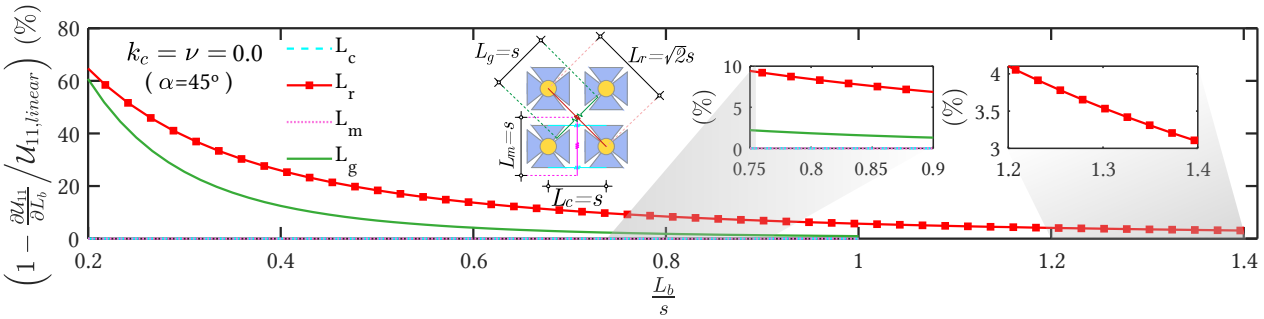

(a) Deviation of the HM isotropy ratio with the lenght of each bond L_b: uni-axial deformation $\mathbf{H_{11}}$

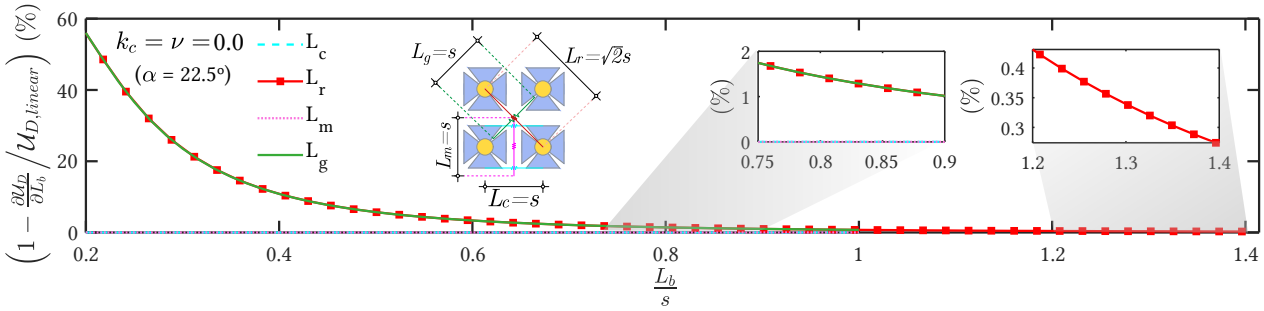

(b) Deviation of the HM isotropy ratio with the lenght of each bond L_b: deviatoric deformation $\mathbf{H_D}$

Figure 7: Relative deviations of the HM isotropy ratio in function of the bonds length L_b , $b = \{c, m, r, g\}$. PS hypothesis with a $\nu = 0.0$, a $k_c = 0$ and a deformation level of 10% were considered for: (a) $\mathbf{H}_{11}$ deformation ($\alpha = 45$) and (b) $\mathbf{H}_{\mathsf{D}}$ deformation ($\alpha = 22.5$).

5. Numerical applications

In this section, the proposed geometrically non-linear HM is applied for the study of two elastic PE problems. In the first problem, the potential of the HM concept as a numerical calculation tool is demonstrated for elastic non-linear and static 2D problems. A solid domain subjected to a non-homogeneous load is studied and the response considering an auxetic or standard material is discussed. The results of the HM are compared with a standard FE using COMSOL Multiphysics. In the second problem, the HM is designed to produce a mechanical response that approximates the complex macro-behaviour found for an auxetic foam under an homogeneous deformation $\mathbf{H}_{11}$. Both experimental and analytical data available in the literature are included in the analysis. At last, further insights on the topology design of the HM are addressed.

5.1. Plane strain thick solid domain under vertical load

The elastic response of a solid domain with dimensions of $1.0 \times 0.5\,\mathrm{m}^2$ (length×height) is investigated and it is assumed that it represents the cross-section of a thick layer of material. The bottom edge of the domain is clamped and the remaining edges are free. A centred load of $600\,kN$ is uniformly distributed over a length of 0.1m with the aim of representing a concentrated action. A plane-strain (PE) problem is considered to compare the solution of the proposed HM with the one obtained with an homogeneous FE continuum. Two materials with a shear modulus of $G = 100$ MPa are investigated, i.e.: (i) an auxetic material with a Poisson's ratio of $\nu = -0.99$, and (ii) a non-auxetic material with a Poisson's ratio of $\nu = 0.1$. Linear quadrilateral FEs were adopted and a structured and regular 80×40 grid FE mesh was defined. For the HM model, a intermolecular distance of $s = 0.0125$m (Fig. 5) was adopted to guarantee the uniformity of discretization between approaches and the objectivity of the comparison.

Results are given in Fig. 8 and include maps for vertical displacements (v), Cauchy-Green deformation (Σ^{σ}_{11}) and Cauchy-stress (Σ^{σ}_{11}) along the global x direction. For both materials, an excellent agreement is found for the vertical displacement map (Fig. 8a) between the HM and the FE continuum. The Green-Lagrangian strain E_{11} (Fig. 8b) and Cauchy stress Σ^{σ}_{11} maps (Fig. 8c) are also generally identical except in the vicinity of the load application.

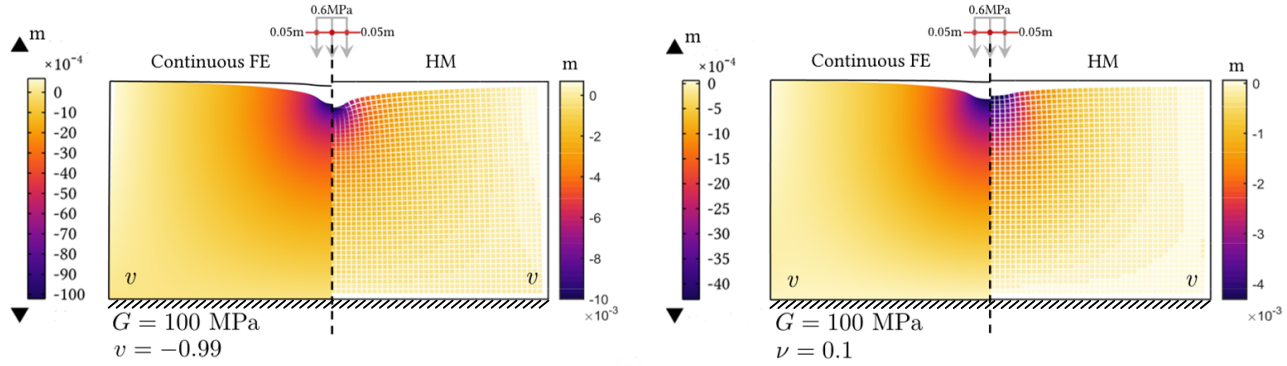

(a) Vertical displacement v map and deformed shape (scale factor of 10)

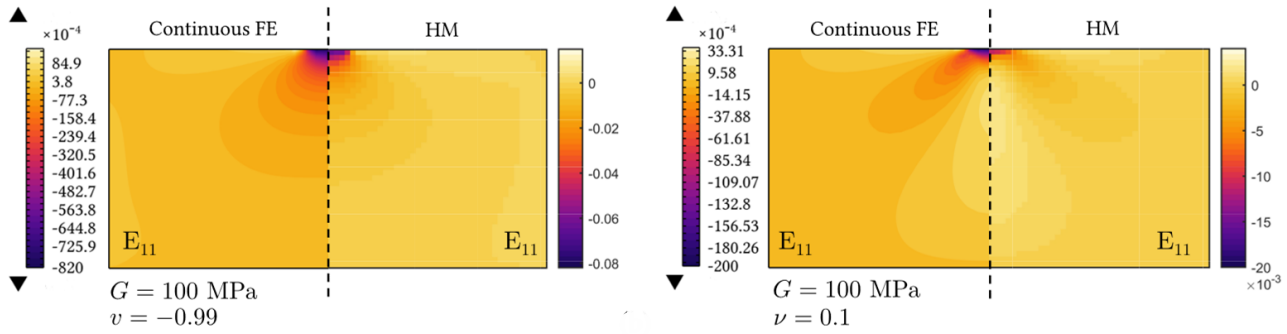

(b) Green-Lagrangian strain E_{11} map

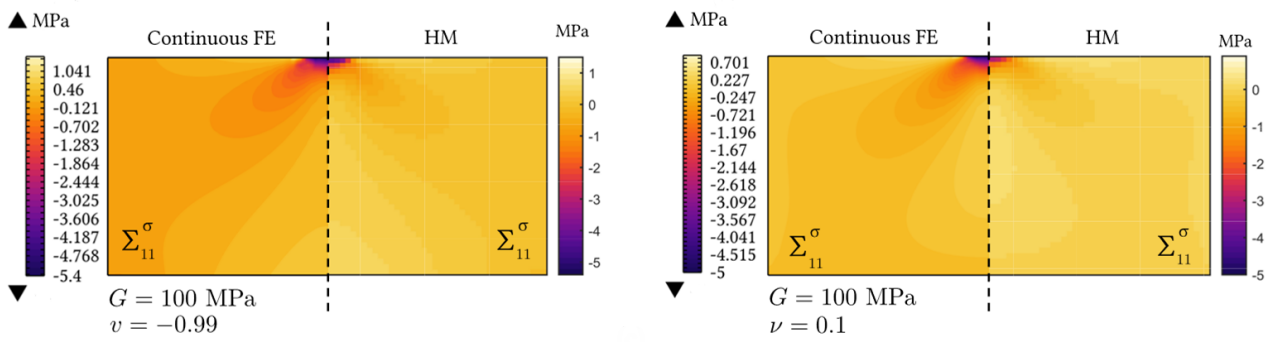

(c) Cauchy stress Σ_{11}^{σ} map

Figure 8: Numerical results of a FE continuum vs HM model for an auxetic ($G = 100$ MPa and $\nu = -0.99$) and non-auxetic ($G = 100$ MPa and $\nu = 0.1$) material: (a) vertical displacement v map and deformed shape (scale factor of 10); (b) Green-Lagrangian strain E_{11} map; and (c) Cauchy stress Σ_{11}^{σ} map.

This difference is well observed through the profiles of E_{11} and Σ_{11}^{σ} for the mid-section of the domain depicted in Fig. 9(b,c). This discrepancy is consequence of the stress concentration that occurs in the FE model. The peaks for the stress and strain values around the load zone are unseen in the HM model since a local spatial averaging is conducted, hence leading to lower values. Such averaging step, which is dependent on the characteristic length of the molecule, is similar to the approach followed already in atomistic models [63]. From

Fig. 9b, it can be also observed that higher deviations are found for the auxetic material. Here, it is important to address that the elasticity terms for the bonds of the auxetic HM are computed according to a Cosserat continuum. Differently, the FE model is based on a Cauchy continuum that disregards the micropolar deformation. Therefore, in the vicinity of the load application whereas larger micro-rotations are found (Fig. 8)a, the HM provides a stiffer response in comparison to the FE model.

From Fig. 9c it is verified that both the FE and the HM models are able to reproduce a similar response near the bottom clamped edge and for both the standard and auxetic materials. For the auxetic case, the applied load contracts the material which is averted by the bottom boundary condition. The response depicted for the Σ^{σ}_{11} in Fig. 9c agrees with the physical sense since in the clamped boundary, in order to react to the contraction of the HM, tensile stresses are generated. The modelling of such perfect adhesion causes this effect that is unseen in the standard material.

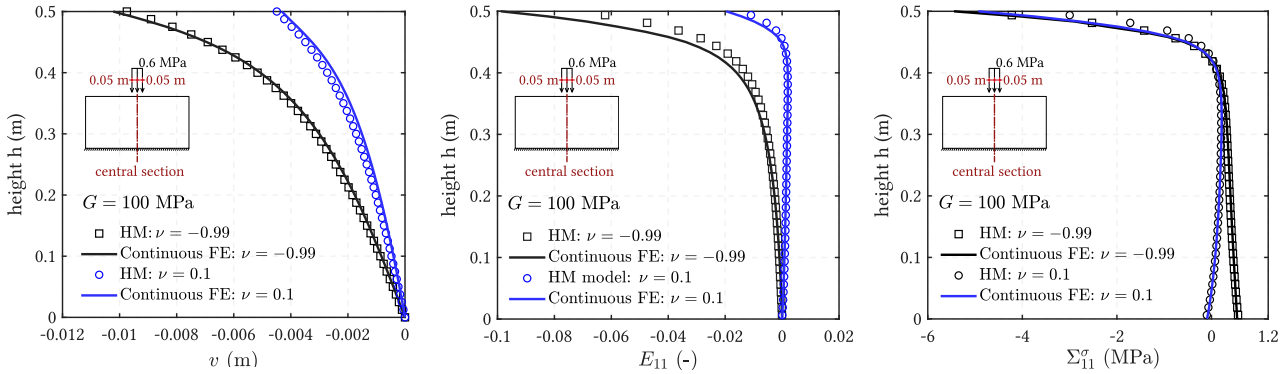

(a) Vertical displacement v (b) Green-Lagrangian strain E_{11} (c) Cauchy stress Σ^{b}_{11}

Figure 9: Mid-section profiles of (a) vertical displacement v, (b) Green-Lagrangian strain E_{11}, and (c) Cauchy-stress Σ^{σ}_{11} for both the non-auxetic and auxetic materials.

5.2. Mechanical response of isotropic and auxetic foams

Efficient methods that predict the mechanical response of auxetic materials under large deformations are important in several fields of application [65, 66]. Attention is here devoted to the case of auxetic foams, in which a nonlinear mechanical response is observed under large deformations [61].The internal auxetic cell of the foam drives the macro-response, which is governed by a change in entropy [67]. To reproduce such behaviour, multi-scale methods [59, 60, 68] and analytical phenomenological models, such as the Blatz-Ko [52] and related

hyperelastic constitutive models [54], are generally pursued. Data-driven procedures seem also a valid alternative when analytical models fail to be accurate [69, 70] and have been also successfully applied for the study of anisotropic foams through a continuum-approach [71].

In specific, the proposed HM is applied to study the response of auxetic foams according to the works of Choi and Lakes [61]. The foam under investigation is auxetic and isotropic [61], however foams can be rather anisotropic due to its complex and random micro-structure [71]. Under a uni-axial deformation, the modelling of the mechanical response of auxetic foams is generally based on analytical relationships. In the seminal works by *Blatz* and *Ko* [52], the relation between longitudinal λ_{11} and transverse λ_{22} stretch is found for a foam subjected to a tensile test. This relation is found as $\lambda_{22}(\lambda_{11}) = \lambda_{11}^{-\nu_0}$ and the Poisson's ratio varies according to Eq.(52):

$$\nu(\lambda_{11}) = -\frac{\varepsilon(\lambda_{11})}{\varepsilon_{11}(\lambda_{11})} = \frac{1-\lambda_{11}^{-\nu_0}}{\lambda_{11}-1} \tag{52}$$

in which ν_0 is the initial Poisson's ratio of the material. This expression is monotonic and unable to capture a sign change for the Poisson's ratio, which is inconsistent with experimental evidence on auxetic foams in the range of large (finite) deformations. The auxetic property of foams is lost after a deformation threshold, as addressed in Crespo et al. [55]: *"auxetic foams behave in an auxetic manner only up to certain deformation level"*. To cope with the latter, *Ciambella & Saccomandi* [54] proposed the following modification:

$$\nu(\lambda_{11}) = -1 - \frac{\nu_0(\lambda_{11}-1)}{(1+\pi^2\nu_0^2(\lambda_{11}-1)^2)^q} \tag{53}$$

in which q ≥ 0.5 and depends on the critical stretch λ_I for which, in a tensile test, the foam stops expanding laterally and occurs the onset of contraction. The parameters λ_I and ν_0 are thus required as input. This analytical expression [54] has a phenomenological character since the change of Poisson's ratio is directly governed by the critical stretch λ_I. The proposed HM is elastic, hence unable to describe the change of the constitutive relationship through ad-hoc parameters found by experiments. Instead, the topology of the molecule is designed to approximate the macro-response of the foam. This is achieved by selecting the lengths L_c , L_r , L_m , L_g for bonds, the size a of the atoms, and the interatomic distance s.

To attest the potential of the HM to reproduce this effect, the data from *Choi* and *Lakes* experiments [61] are used. The authors performed tension-compression uni-axial tests on isotropic and re-entrant foams. These data allowed to provide the elastic parameters required for the calibration of both the analytic and the HM model, i.e. a Poisson's ratio of $\nu = -0.53$ and a critical stretch $\lambda_I = 1.33$. To this aim, a discretization of 4×4 molecules was assumed and an incremental displacement applied in uni-axial tension ($\mathbf{H}^{11} = \Delta\ (\boldsymbol{e}^1 \otimes \boldsymbol{e}^1)$) and compression ($\mathbf{H}^{11} = -\Delta\ (\boldsymbol{e}^1 \otimes \boldsymbol{e}^1)$). Fig. 10a and Fig. 10b present, respectively, the uni-axial Cauchy stress with the stretch response and the relation between transverse λ_{22} and longitudinal λ_{11} stretch terms. The calibration of the molecular topology has been achieved aiming to reproduce the transversal behaviour of the foam with good approximation. The values found are $k_c = 0.3G, L_c = D, L_r = a\sqrt{2}, L_m = 2a, L_g = 0.4a$.

The results in terms of stress-stretch curve in tension show a good agreement with the experiments, but some differences are yet found in compression. It is noteworthy to address that both the analytical and the HM model feature a response that is symmetric in tension and compression. In fact, under significant compression stretch levels, it is expected that the contacts offered by the micro-structure of the foam can provide an important contribution to the mechanical response. To reproduce such densification effect and to better approximate the results offered by the HM, the stiffness of compressed bonds can be increased. This requires to describe an inelastic material constitutive response, which is beyond the scope of this study but may be investigated in a future work. In the main, the HM is able to catch the change of Poisson's sign even if is based on an elastic formulation. Differently from hyperelastic constitutive-based models [52, 54], the mechanical response offered by the HM is governed by the non-linear geometry effects of the foams micro-structure rather than by a constitutive-based approach.

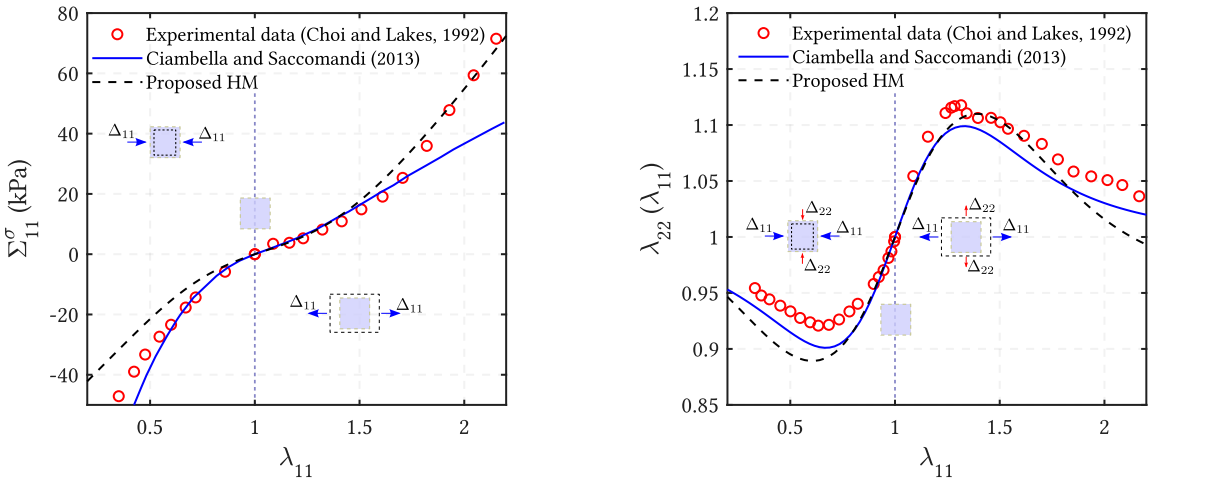

(a) Cauchy stress Σ_{11}^{b} with the longitudinal stretch λ_{11}

(b) Vertical stretch λ_{22} with the longitudinal stretch λ_{11}

Figure 10: Comparison between the proposed HM and the analytical [54] model with experiments data of an auxetic foam under uni-axial loading [61]:(a) Cauchy stress σ_{11}, and (b) evolution of the vertical (transverse) stretch λ_{22} with the longitudinal stretch λ_{11}.

This investigation allows to demonstrate (1) how the topology of the HM can be designed to reproduce a solid with a mechanical behaviour that resembles with the macro-response of the foam; and (2) how the HM can be, as direct extension, a data-driven calculation tool for auxetic isotropic foams. On one hand, the topology of the HM is tailored to obtain a mechanical response that approximates the macro-behaviour of the foam, hence precluding the need of explicitly modelling its micro-structure. The problem resorts to a topology finding process, alike to the one that may be used to design a novel metamaterial with a basic unit-cell given by the heuristic molecule. On the other hand, the HM can be calibrated and used as a calculation tool for the mechanical study of foams, whose formulation relies on an energy approach, rather than explained by a statistical homogenized theory [72, 73].

5.3. Further insights on the response of isotropic foams

The application of the proposed HM model for the study of foams proved that its topology can be adapted to approximate the non-linear response of foams under large deformations. The macro-response of the molecule is affected by changing the size of atoms and the inter-atomic distance. This is somehow associated with the real behaviour of meta-materials whose mechanical response depends on the micro-structure arrangement. Such topology adaptation may allow to design different materials and may be seen as a form-finding process.

Within this perspective, the comparison between the HM and the analytical model from Ciambella and Saccomandi [54] is extended. A foam with membrane-alike shape and considering four initial Poisson's values $\nu_0 = \{-1, -0.5, 0.0, 0.2\}$ is assumed for this discussion. A PS model of 4×4 molecules with unit area and subjected to a uni-axial tension stretch was assumed. A calibration of the molecule topology was conducted in order to fit the results provided by Eq.(53) for a critical stretch $\lambda_I = 2$ [54] and the comparison is presented in Fig. 11. In specific, the length of bonds and the stiffness of the media (through k_c) were modified to fit the elastic strain energy of the foam and respecting the conditions of Eq.(26). The parameters found are described in each subplot of Fig. 11. The HM approximates the analytical prediction for each initial Poisson ratio ν_0 and is able to show the inversion of the transversal response of the material as initially hypothesized. However, some differences are visible for $\lambda_{11} \geq 1.25$ and are well marked for $\lambda_{11} \geq 1.4$.

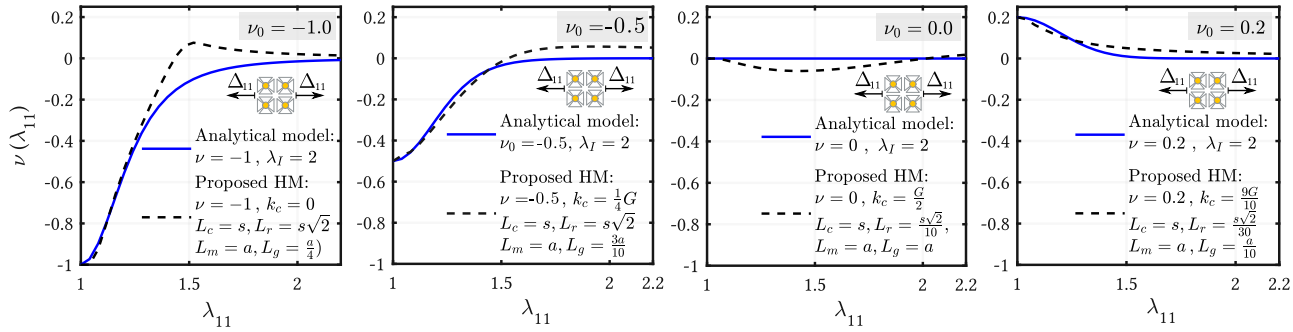

(a) Poisson's ratio ν in function of the longitudinal stretch λ_{11}

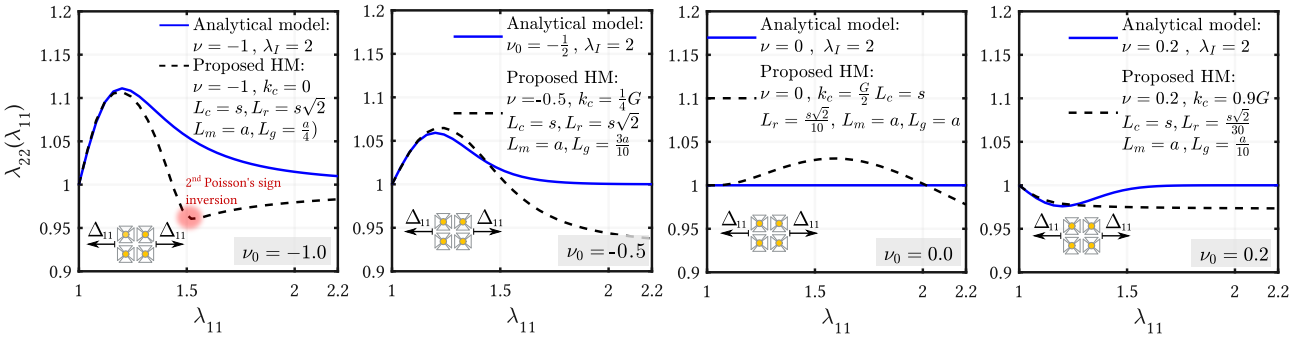

(b) Vertical (transverse) stretch λ_{22} in function of the longitudinal stretch λ_{11}

Figure 11: Proposed HM model vs analytical model from Ciambella and Saccomandi [54]: (a) Poisson's ratio ν in function of the uni-axial tensile stretch λ_{11}; and (b) transverse stretch λ_{22} in function of the uni-axial stretch λ_{11}.

Thanks to the concept of HM, it is rather possible to design a hyperelastic metamaterial that may feature a similar macro-response of a foam, and yet with a different topology than the microstructure observed in foams. Furthermore, non-standard mechanical properties may have ground for further practical investigation. For instance, the auxeticity and quasi-isotropy under large deformations of the HM, as well as the effect highlighted in Fig. 11b, in which a molecule with an initial Poisson of $\nu = -1.0$, critical stretch $\lambda_I = 2$ and a topology defined by $L_c = s,\ L_r = s\sqrt{2},\ L_m = a,\ L_g = \frac{a}{4}$ shows two inversions for the Poisson's sign, differently from the response of an auxetic foam that displays only one inversion. It can be also recalled that the HM concept may be extended to calculate and to design different metamaterials, at least for physically admissible geometries. In such cases, the HM can be considered as a discrete material with an established periodic micro-structure composed of slender parts (the bonds) that connect stiffer portions (the atoms).

6. Final remarks

A two-dimensional molecular model has been formulated according to a finite strain theory. The basic unit-cell was designed according to a heuristic molecule approach [42], which consists of four rigid atoms placed in a regular pattern and interconnected by five types of centred and non-centred bonds. Under such assumption, this specific heuristic molecule (HM) can describe the mechanical response of a wide variety of elastic materials. The HM is frame indifferent and, differently from other models that resort on particles, the molecular topology is easily parametrisable to give an arbitrary shape to the atoms and different characteristics to the elastic bonds.

The numerical performance of the HM was tested for planar static problems by comparing the response of a standard and an auxetic material under a non-homogeneous deformation field. At a macro-scale, an excellent agreement was found with a FE continuum using COMSOL Multipyshics, for which displacement, strain and stress fields were accounted. To this aim, a measure of stress was introduced even if this aspect can be somewhat debatable within a discrete modelling framework. Anyway, it can be useful to explore the homogenization step performed over the HM domain in a micro-macro strategy, as well as to extend the HM with non-linear stress-strain laws that are generally provided through experimental characteri-

zation tests. Interesting observations were also found by applying the model to reproduce the experiments by Lakes [28] on auxetic foams under large displacements. The topology parametrization of the HM allowed to find bespoke sizes for bonds and atoms that approximates the macro-mechanical response of the foam. Results give an interesting perspective on how a molecular model, which is defined at a macro-scale, is also able to reproduce local effects without the need of a strenuous direct numerical simulation that requires the modeling of the internal microstructure of foams. A geometric-based (or physical) cause for the non-linear response of foams is kept, differently to current analytical models for foams [54] or hyperelastic materials in general [50–53] that are implicitly related with a constitutive standpoint.

The formulation of the HM pursued a methodological attitude that is supported by aspects confirmed by experiments. Such physical-driven approach narrows the admissible range of Poisson's values for materials under investigation, in specific $-1 \leq \nu \leq \frac{1}{3}$ and $-1 \leq \nu \leq \frac{1}{4}$ for PS and PE cases, respectively. Nonetheless, it also allows to extend the conclusions beyond a pure numerical application. The positivity of elasticity stiffness for bonds and the assignment of a physical shape to atoms give a wide possibility of controlling the topology of the molecule to configure and design various meta-materials. Moreover, the HM can be used for the modelling of: (1) materials with an auxetic response $-1 \leq \nu < 0$; (2) materials with fully elastic isotropy under small strains or with a remarkable quasi-isotropy under large deformations, which overcomes one of the main shortcoming of many discrete-based approaches [3]; and (3) ultra-soft auxetic material with initial $\nu = -1$ that shows two inversions for the Poisson's sign under large deformations.

At last, two remarks on future studies are addressed. As first, it is remarkable that the HM approach can serve as a calculation tool. This model can constitute a basis for future developments related with physical non-linearity, with damage onset, fracture propagation and extension to the three-dimensional case. Secondly, and in the realm of an applicative framework, a future research dedicated only to the topology-physical aspect of the HM can be pursued. Different atoms arrangements can be analysed, either following a regular lattice, such as hexagonal or rectangular, or through a random spacial distribution. In this study, a random organization of the lattice was unexplored given that the expected target, also

from an engineering point of view, is to design artificial materials that must necessarily be "constructed" to reach a regularly periodic internal organization. Additionally, and within the aim of investigating the derived physical properties at the macro-scale, other topologies can be defined by considering an atom with different shape or types and number of bonds. For instance, by adapting the interatomic distances between adjoining atoms it is possible to create a meta-material with bandgaps [74, 75] or with varying wavelengths for dissipative purposes [76–78]; the auxetic property of the HM can be used to design energy dissipating layers for impact mitigation systems [77, 79]; the material properties for the bonds can be modified aiming at a negative hygroscopic expansion ratio [80], among others. From a production standpoint, the possibility of physically reproducing the HM through a discrete assembly or a continuous one using additive manufacturing can be explored. In this regard, the use of rigid atoms and spring-based bonds may fit well within an incremental and discrete assembly, which appears to have clear advantages in terms of cost and scalability as addressed in [81].

7. Acknowledgements

The first author gratefully acknowledges the funding of the Ministry of University and Research, MUR, Italy, within the program PON Research and Innovation 2014-2020, and research project code (CUP) D45F21003530001: *'Multiphysics of innovative micro-structured materials with adaptive mechanical properties for the safety and optimal performance of constructions'*.

Appendix A. Deformation gradient tensor for the heuristic molecule

Continuum-related quantities such as the stress and strain tensors can be associated to the discrete heuristic molecule. The bridge between these approaches is inherently achieved by assuming a local averaging within the unit-cell domain of each molecule Ω. Here, the second-order deformation gradient tensor $\mathbf{F}$ is found for the HM, for which molecules are assumed to have a squared shape with size s in the reference (undeformed) configuration. Furthermore, a linear interpolation for the deformation within Ω is adopted. From the global

coordinates $\mathbf{x}^i = \{x^{n_i}, y^{n_i}\}^T$ of atoms $i = 1, 2, 3, 4$ of a generic molecule, as depicted in Fig. 4, and the corresponding planar displacements $\{u^i, v^i\}^T$, the tensor $\mathbf{F}$ is given by:

$$\mathbf{F} = \begin{bmatrix} F_{11} & F_{12} \\ F_{21} & F_{22} \end{bmatrix}$$

$$\begin{aligned} F_{11}(x,y) &= \tfrac{1}{s}\Big((1-\tfrac{y-y^{n_1}}{s})(u^{n_2}-u^{n_1}) + (1-\tfrac{y^{n_3}-y}{s})(u^{n_3}-u^{n_4})\Big) + 1 \\ F_{12}(x,y) &= \tfrac{1}{s}\Big((1-\tfrac{x-x^{n_1}}{s})(u^{n_4}-u^{n_1}) + (1-\tfrac{x^{n_2}-x}{s})(u^{n_3}-u^{n_2})\Big) \\ F_{21}(x,y) &= \tfrac{1}{s}\Big((1-\tfrac{y-y^{n_1}}{s})(v^{n_2}-v^{n_1}) + (1-\tfrac{y^{n_3}-y}{s})(v^{n_3}-v^{n_4})\Big) \\ F_{22}(x,y) &= \tfrac{1}{s}\Big((1-\tfrac{x-x^{n_1}}{s})(v^{n_4}-v^{n_1}) + (1-\tfrac{x^{n_2}-x}{s})(v^{n_3}-v^{n_2})\Big) + 1 \end{aligned} \tag{A.1}$$

in which x and y are planar global coordinates of a point inside the molecular domain Ω. Therefore, the deformation gradient $\mathbf{F}$ can be computed in the centre of each molecule such that $(x, y) \to (x^c, y^c)$ and:

$$x^c = \sum_{i=1}^{4} \frac{x^{n_i}}{4} \quad , \quad y^c = \sum_{i=1} \frac{y^{n_i}}{4} \tag{A.2}$$

Appendix B. Linearized and non-linear strain energies

The linearized and non-linear strain energies for the proposed heuristic molecule are addressed. Note that the individual contribution of each bond type is well recognized since different terms for the bond length (L_c, L_r, L_m and L_g) and stiffness (k_c, k_r, k_n, and k_g) have been provided and are consistent with the notation used throughout the manuscript.

The linearized strain energies for the considered homogeneous deformations fields are given in Eq. (B.1).

$$\begin{aligned} \mathcal{U}_{11_\xi} &= \Delta^2 \left(3\,k_c + 2\,k_g + k_m + 3\,k_r + \cos(4\,\alpha)\,(k_c + 2k_g - k_m - k_r)\right) \\ \mathcal{U}_{D_\xi} &= 4\,\Delta^2 \left(k_c + 2\,k_g + k_m + k_r + \cos(4\,\alpha)\,(k_m + k_r - k_c - 2\,k_g)\right) \\ \mathcal{U}_{H_\xi} &= 8\Delta^2\Big(k_c + k_r\Big) \end{aligned} \tag{B.1}$$

The non-linear strain energy terms are given as follows. For the uni-axial deformation

mode $\mathbf{H_{11}}$ it reads as:

$$\begin{aligned}\mathcal{U}_{11} = L_c k_c \left(4L_c + 4\Delta + 4\Delta^2/L_c - 2\sqrt{A_c - B_c} - 2\sqrt{A_c + B_c}\right) + \\ L_r\, k_r \left(2\,L_r + 4\,\Delta^2/L_r + 2\,\sqrt{2}\,\Delta - \sqrt{A_r - B_r} - \sqrt{A_r + B_r}\right) + \\ L_g\, k_g \left(4\,L_g + 8\,\Delta^2/L_g - \sqrt{A_g - B_g} - \sqrt{A_g - C_g} - \sqrt{A_g + C_g} - \sqrt{A_g + B_g}\right) + \\ L_m\, k_m \left(4\,L_m + 4\,\Delta^2/L_m - \sqrt{A_m - B_m} - \sqrt{A_m - C_m} - \sqrt{A_m + C_m} - \sqrt{A_m + B_m}\right)\end{aligned} \tag{B.2}$$

in which:

$$\begin{aligned} A_c &= 2\,L_c\,\Delta + {L_c}^2 + 2\,\Delta^2 \quad ; \quad B_c = 2\,\Delta^2\,\cos(2\,\alpha) + 2\,L_c\,\Delta\,\cos(2\,\alpha) \\ A_r &= {L_r}^2 + 4\,\Delta^2 + 2\,\sqrt{2}\,L_r\,\Delta \quad ; \quad B_r = 4\,\Delta^2\,\sin(2\,\alpha) + 2\,\sqrt{2}\,L_r\,\Delta\,\sin(2\,\alpha) \\ A_m &= {L_m}^2 + 2\,\Delta^2 \quad ; \quad B_m = 2\,\Delta^2\,\cos(2\,\alpha) + 2\,L_m\,\Delta\,\sin(2\,\alpha) \\ C_m &= 2\,\Delta^2\,\cos(2\,\alpha) - 2\,L_m\,\Delta\,\sin(2\,\alpha) \\ A_g &= {L_g}^2 + 4\,\Delta^2 \quad ; \quad B_g = 4\,\Delta^2\,\sin(2\,\alpha) + 2\,\sqrt{2}\,L_g\,\Delta\,\cos(2\,\alpha) \\ C_g &= 4\,\Delta^2\,\sin(2\,\alpha) - 2\,\sqrt{2}\,L_g\,\Delta\,\cos(2\,\alpha) \end{aligned}$$

For the deviatoric deformation mode $\mathbf{H_D}$:

$$\begin{aligned}\mathcal{U}_D = 2L_c\,k_c \left(2\,L_c + 4\,\Delta^2/L_c - \sqrt{C_c - D_c} - 2\sqrt{C_c + D_c}\right) + L_r\,k_r \left(2L_r + \right. \\ \left. 8\,\Delta^2/L_r - \sqrt{D_r - F_r} - \sqrt{D_r + F_r}\right) + 2L_m\,k_m \left(2L_m + 4\,\Delta^2/L_m - \sqrt{D_m - F_m} - \sqrt{D_m + F_m}\right) + \\ 2L_g\,k_g \left(2\,L_g + 8\,\Delta^2/L_g - \sqrt{D_g - F_g} - \sqrt{D_g + F_g}\right)\end{aligned} \tag{B.3}$$

in which:

$$\begin{aligned} C_c &= {L_c}^2 + 4\,\Delta^2 \quad ; \quad D_c = 4\Delta\,L_c \sin(2\,\alpha) \\ D_r &= {L_r}^2 + 8\,\Delta^2 \quad ; \quad F_r = 4\,\sqrt{2}\Delta\,L_r \cos(2\,\alpha) \\ D_m &= {L_m}^2 + 4\,\Delta^2 \quad ; \quad F_m = 4\,\Delta\,L_m \cos(2\,\alpha) \\ D_g &= {L_g}^2 + 8\,\Delta^2 \quad ; \quad F_g = 4\,\sqrt{2}\Delta\,L_g \sin(2\,\alpha) \end{aligned}$$

For the hydrostatic deformation mode $\mathbf{H_H}$:

$$\mathcal{U}_H = 8\Delta^2 k_c + 4k_m\Big({L_m}^2 - L_m\sqrt{D_m} + 2\Delta^2\Big) + 2k_r\Big({L_r}^2 + 2\sqrt{2}\,\Delta\,L_r + 4\,\Delta^2 - L_r\sqrt{D_r + 4\sqrt{2}\,L_r\,\Delta}\Big) + 4k_g\Big({L_g}^2 + 4\Delta^2 - L_g\sqrt{D_g}\Big) \quad \text{(B.4)}$$

Appendix C. Partial derivatives for deformation mode $\mathbf{H_{11}}$

The partial derivatives of the energy associated with $\mathbf{H_{11}}$ deformation mode are given next according to the variation of the length for each bond (see Fig. 1). For the vertical and horizontal (type-c, cyan) bonds:

$$\frac{\partial \mathcal{U}_{11}}{\partial L_c} = k_c\Big(8\,L_c + 4\,\Delta - 2\sqrt{A_c - B_c} - 2\sqrt{A_c + B_c} - \frac{L_c\,F_c}{\sqrt{A_c - B_c}} - \frac{L_c\,G_c}{\sqrt{A_c + B_c}}\Big) \quad \text{(C.1)}$$

in which:

$$F_c = 2\,L_c + 2\,\Delta - 2\,\Delta\,\cos(2\,\alpha) \quad ; \quad G_c = 2\,L_c + 2\,\Delta + 2\,\Delta\,\cos(2\,\alpha)$$

For the diagonal (type-r, red) bonds:

$$k_r\Big(4\,L_r + 2\sqrt{2}\,\Delta - \sqrt{A_r - B_r} - \sqrt{A_r + B_r} - \frac{L_r\,(L_r + F_r)}{\sqrt{A_r - B_r}} - \frac{L_r\,(L_r + G_r)}{\sqrt{A_r + B_r}}\Big) \quad \text{(C.2)}$$

in which:

$$F_r = \sqrt{2}\,\Delta - \sqrt{2}\,\Delta\,\sin(2\,\alpha) \quad ; \quad G_r = \sqrt{2}\,\Delta + \sqrt{2}\,\Delta\,\sin(2\,\alpha)$$

For the vertical and horizontal shear (type-m, magenta) bonds:

$$\frac{\partial \mathcal{U}_{11}}{\partial L_m} = k_m\Big(8\,L_m - \sqrt{A_m - B_m} - \sqrt{A_m - C_m} - \sqrt{A_m + C_m} - \sqrt{A_m + B_m} - \frac{L_m\,G_m}{2\sqrt{A_m - B_m}} - \frac{L_m\,G_m}{2\sqrt{A_m + C_m}} - \frac{L_m\,H_m}{2\sqrt{A_m - C_m}} - \frac{L_m\,H_m}{2\sqrt{A_m + B_m}}\Big) \quad \text{(C.3)}$$

in which:

$$G_m = 2\,L_m - 2\,\Delta\,\sin(2\,\alpha) \quad ; \quad H_m = 2\,L_m + 2\,\Delta\,\sin(2\,\alpha)$$

For the diagonal shear (type-g, green) bonds:

$$\frac{\partial \mathcal{U}_{11}}{\partial L_g} = k_g \Big(8\,L_g - \sqrt{A_g - B_g} - \sqrt{A_g - C_g} - \sqrt{A_g + C_g} - \sqrt{A_g + B_g} - \frac{L_g\,k_g\,G_g}{2\,\sqrt{A_g - B_g}} - \frac{L_g\,G_g}{2\,\sqrt{A_g + C_g}} - \frac{L_g\,H_g}{2\,\sqrt{A_g - C_g}} - \frac{L_g\,H_g}{2\,\sqrt{A_g + B_g}}\Big) \quad \text{(C.4)}$$

660 $$G_g = 2\,L_g - 2\,\sqrt{2}\,\Delta\,\cos(2\,\alpha) \quad ; \quad H_g = 2\,L_g + 2\,\sqrt{2}\,\Delta\,\cos(2\,\alpha)$$

Appendix D. Partial derivatives for deformation mode $\mathbf{H_D}$

The partial derivatives of the energy associated with the deviatoric $\mathbf{H_D}$ deformation are given next according to the variation of the length for each bond (see Fig. 1). For the vertical and horizontal (type-c, cyan) bonds:

$$\frac{\partial \mathcal{U}_{12}}{\partial L_c} = 2k_c\Big(4L_c - \sqrt{D_c - F_c} - \sqrt{D_c + F_c}\Big) - L_c\,k_c\left(\frac{(2\,L_c - F_c/L_c)}{\sqrt{D_c - F_c}} + \frac{(2\,L_c + F_c/L_c)}{\sqrt{D_c + F_c}}\right) \quad \text{(D.1)}$$

in which:

$$D_c = {L_c}^2 + 4\,\Delta^2 \quad ; \quad F_c = 4\Delta\,L_c \sin(2\,\theta)$$

For the diagonal (type-r, red) bonds:

$$\frac{\partial \mathcal{U}_{12}}{\partial L_r} = k_r\Big(2L_r - \sqrt{C_r - D_r} - \sqrt{C_r + D_r}\Big) - L_r\,k_r\left(\frac{(2\,L_r - D_r/L_r)}{\sqrt{C_r - D_r}} + \frac{(2\,L_r + D_r/L_r)}{\sqrt{C_r + D_r}}\right) \quad \text{(D.2)}$$

in which:

665 $$C_r = {L_r}^2 + 8\,\Delta^2 \quad ; \quad D_r = 4\,\sqrt{2}\Delta\,L_r \cos(2\,\alpha)$$

For the horizontal and vertical shear (type-m, magenta) bonds:

$$\frac{\partial \mathcal{U}_{12}}{\partial L_m} = 2k_m\Big(4L_m - \sqrt{D_m - F_m} - \sqrt{D_m + F_m}\Big) - L_m\, k_m \left(\frac{(2\,L_m - F_m/L_m)}{\sqrt{D_m - F_m}} + \frac{(2\,L_m + F_m/L_m)}{\sqrt{D_m + F_m}}\right) \quad \text{(D.3)}$$

in which:

$$D_m = {L_m}^2 + 4\,\Delta^2 \quad ; \quad F_m = 4\,\Delta\, L_m \cos(2\,\alpha)$$

For the diagonal shear (type-g, green) bonds:

$$\frac{\partial \mathcal{U}_{12}}{\partial L_g} = 2k_g\Big(4L_g - \sqrt{D_g - F_g} - \sqrt{D_g + F_g}\Big) - L_g\, k_g \left(\frac{(2\,L_g - F_g/L_g)}{\sqrt{D_g - F_g}} + \frac{(2\,L_g + F_g/L_g)}{\sqrt{D_g + F_g}}\right) \quad \text{(D.4)}$$

in which:

$$D_g = {L_g}^2 + 8\,\Delta^2 \quad ; \quad F_g = 4\sqrt{2}\Delta\, L_g \sin(2\,\alpha)$$

References

[1] Poisson CLMH. Mémoire sur les équations générales de l'équilibre et du mouvement des corps solides élastiques et des fluides. Journal de l'École Polytechnique 1831;3:1–174.

[2] Cauchy AL. Sur l'équilibre et le mouvement d'un système de pointsmatériels sollicités par des forces d'attraction ou de répulsion mutuelle. Exercices de Mathématiques 1828;3:188–213.

[3] Capecchi D, Ruta G, Trovalusci P. From classical to Voigt's molecular models in elasticity. Archive for History of Exact Sciences 2010;64:525–59. doi:10.1007/s00407-010-0065-y.

[4] Stakgold I. The Cauchy relations in a molecular theory of elasticity. Quarterly of Applied Mathematics 1950;8(2):169–86. doi:10.1090/qam/36650.

[5] Voigt W. Theoretische studien über die elasticitätsverhältnisse der krystalle. i. Abhandlungen der Königlichen Gesellschaft der Wissenschaften in Göttingen 1887;34:3–52.

[6] Voigt W. L'état actuel de nos connoissances sur l'élasticité des cristaux. In: Guillaume CE, Poincaré L, editors. Rapports présentés au Congrès international de Physique. Paris: Gauthier-Villars; 1900, p. 277–347.

[7] Tanaka H, Shibutani Y. In-plane mechanical behaviors of 2d repetitive frameworks with four-coordinate flexible joints and elbowed beam members. Journal of the Mechanics and Physics of Solids 2009;57:1485–99. doi:10.1016/j.jmps.2009.06.001.

[8] Wang F, Sigmund O, Jensen JS. Design of materials with prescribed nonlinear properties. Journal of the Mechanics and Physics of Solids 2014;69:156–74. doi:10.1016/j.jmps.2014.05.003.

[9] Cabras L, Brun M. A class of auxetic three-dimensional lattices. Journal of the Mechanics and Physics of Solids 2016;91:56–72. doi:10.1016/j.jmps.2016.02.010.

[10] Nikolić M, Karavelić E, Ibrahimbegovic A, Miščević P. Lattice Element Models and Their Peculiarities; vol. 25. Springer Netherlands; 2018. ISBN 0123456789. doi:10.1007/s11831-017-9210-y.

[11] Kumar D, Poh LH, Quek ST. Isogeometric shape optimization of missing rib auxetics with prescribed negative Poisson's ratio over large strains using genetic algorithm. International Journal of Mechanical Sciences 2021;193(July 2020):106169. doi:10.1016/j.ijmecsci.2020.106169.

[12] Eremeyev VA, Turco E. Enriched buckling for beam-lattice metamaterials. Mechanics Research Communications 2020;103:103458. doi:10.1016/j.mechrescom.2019.103458.

[13] Turco E, Dell'Isola F, Cazzani A, Rizzi NL. Hencky-type discrete model for pantographic structures: numerical comparison with second gradient continuum models. Zeitschrift für angewandte Mathematik und Physik 2016;67(4):85. doi:10.1007/s00033-016-0681-8.

[14] Christos SD, Vlasis KK. Plane stress problems using hysteretic rigid body spring network models. Computational Particle Mechanics 2017;4(4):429–39. doi:10.1007/s40571-016-0128-1.

[15] Casolo S. Macroscale modelling of microstructure damage evolution by a rigid body and spring model. Journal of Mechanics of materials and Structures 2009;4(3):551–70. doi:10.2140/jomms.2009.4.551.

[16] Casolo S. Macroscopic modelling of structured materials: Relationship between orthotropic cosserat continuum and rigid elements. International Journal of Solids and Structures 2006;43(3):475–96. doi:10.1016/j.ijsolstr.2005.03.037.

[17] Silva LC, Lourenco PB, Milani G. Rigid block and spring homogenized model (HRBSM) for masonry subjected to impact and blast loading. International Journal of Impact Engineering 2017;109:14–28. doi:10.1016/j.ijimpeng.2017.05.012.

[18] Ghaboussi J, Barbosa R. Three-dimensional discrete element method for granular materials. International Journal for Numerical and Analytical Methods in Geomechanics 1990;14(7):451–72. doi:10.1002/nag.1610140702.

[19] Lemos JV. Discrete element modeling of masonry structures. International Journal of Architectural Heritage 2007;1:190–213. doi:10.1080/15583050601176868.

[20] Silling S. Reformulation of elasticity theory for discontinuities and long-range forces. Journal of the Mechanics and Physics of Solids 2000;48(1):175–209. doi:10.1016/S0022-5096(99)00029-0.

[21] Gerstle W, Sau N, Silling S. Peridynamic modeling of concrete structures. Nuclear Engineering and Design 2007;237(12):1250–8. doi:10.1016/j.nucengdes.2006.10.002; 18th International Conference on Structural Mechanics in Nuclear Engineering.

[22] Ballarini R, Diana V, Biolzi L, Casolo S. Bond-based peridynamic modelling of singular and nonsingular crack-tip fields. Meccanica 2018;53:3495–515. doi:10.1007/s11012-018-0890-7.

[23] Diana V, Casolo S. A bond-based micropolar peridynamic model with shear deformability: Elasticity, failure properties and initial yield domains. International Journal of Solids and Structures 2019;160:201–31. doi:10.1016/j.ijsolstr.2018.10.026.

[24] Diana V, Casolo S. A full orthotropic micropolar peridynamic formulation for linearly elastic solids. International Journal of Mechanical Sciences 2019;160:140–55. doi:10.1016/j.ijmecsci.2019.06.036.

[25] Silling SA, Epton M, Weckner O, Xu J, Askari E. Peridynamic states and constitutive modeling; vol. 88. 2007. ISBN 1065900791. doi:10.1007/s10659-007-9125-1.

[26] Sarego G, Le QV, Bobaru F, Zaccariotto M, Galvanetto U. Linearized state-based peridynamics for 2-d problems. International Journal for Numerical Methods in Engineering 2016;108(10):1174–97. doi:10.1002/nme.5250.

[27] Barchiesi E, Spagnuolo M, Placidi L. Mechanical metamaterials: a state of the art. Mathematics and Mechanics of Solids 2019;24(1):212–34. doi:10.1177/1081286517735695.

[28] Lakes RS, Benedict RL. Noncentrosymmetry in micropolar elasticity. International Journal of Engineering Sciences 1982;20:1161–7. doi:10.1016/0020-7225(82)90096-9.

[29] Lakes R. Foam structures with negative poisson's ratio. Science 1987;235:1038–40. doi:10.1126/science.235.4792.1038.

[30] Chan N, Evans KE. Fabrication methods for auxetic foams. Journal of Materials Science 1997;32(22):5945–53. doi:10.1023/A:1018606926094.

[31] Brandel B, Lakes RS. Negative Poisson's ratio polyethylene foams. Journal of Materials Science 2001;36(24):5885–93. doi:10.1023/A:1012928726952.

[32] Soyarslan C, Blümer V, Bargmann S. Tunable auxeticity and elastomechanical symmetry in a class of very low density core-shell cubic crystals. Acta Materialia 2019;177:280–92. doi:10.1016/j.actamat.2019.07.015.

[33] Prawoto Y. Seeing auxetic materials from the mechanics point of view: A structural review on the negative Poisson's ratio. Computational Materials Science 2012;58:140–53. doi:10.1016/j.commatsci.2012.02.012.

[34] Su Y, Xu X, Shi J, Huang G. A 3d mechanism-driven hexagonal metamaterial: Evaluation of auxetic behavior. International Journal of Mechanical Sciences 2021;209. doi:10.1016/j.ijmecsci.2021.106699.

[35] Shen L, Wang Z, Wang X, Wei K. Negative poisson's ratio and effective young's modulus of a vertex-based hierarchical re-entrant honeycomb structure. International Journal of Mechanical Sciences 2021;206:106611. doi:10.1016/j.ijmecsci.2021.106611.

[36] Cheng X, Zhang Y, Ren X, Han D, Jiang W, Zhang XG, et al. Design and mechanical characteristics of auxetic metamaterial with tunable stiffness. International Journal of Mechanical Sciences 2022;223. doi:10.1016/j.ijmecsci.2022.107286.

[37] Grima JN, Alderson A, Evans KE. Auxetic behaviour from rotating rigid units. physica status solidi (b) 2005;242(3):561–75. doi:10.1002/pssb.200460376.

[38] Guo CY, Wheeler L. Extreme poisson's ratios and related elastic crystal properties. Journal of the Mechanics and Physics of Solids 2006;54:690–707. doi:10.1016/j.jmps.2005.11.002.

[39] Gao E, Li R, Fang S, Shao Q, Baughman RH. Bounds on the in-plane poisson's ratios and the in-plane linear and area compressibilities for sheet crystals. Journal of the Mechanics and Physics of Solids 2021;152. doi:10.1016/j.jmps.2021.104409.

[40] Runkel F, Ramstein G, Molinari G, Arrieta AF, Ermanni P. Mechanics of curved-ligament hexachiral metastructures under planar deformations. Journal of the Mechanics and Physics of Solids 2019;125:145–63. doi:10.1016/j.jmps.2018.12.001.

[41] De Cicco S, Ieşan D. A Theory of Chiral Cosserat Elastic Plates. Journal of Elasticity 2013;111(2):245–63. doi:10.1007/s10659-012-9400-7.

[42] Casolo S. A linear-elastic heuristic-molecular modelling for plane isotropic micropolar and auxetic materials. International Journal of Solids and Structures 2021;224(111042). doi:10.1016/j.ijsolstr.2021.111042.

[43] Foce F. La teoria molecolare dell'elasticità. Dalla fondazione ottocentesca ai nuovi sviluppi del XX secolo. Phd thesis; 1995.

[44] Trovalusci P, Capecchi D, Ruta G. Genesis of the multiscale approach for materials with microstructure. Archive of Applied Mechanics 2009;79(11):981–97. doi:10.1007/s00419-008-0269-7.

[45] Cosserat E. Théorie des corps déformables. Librairie Scientifique A. Hermann et Fils; 1909.

[46] Murdoch A. On the relationship between balance relations for generalised continua and molecular behaviour. International Journal of Engineering Science 1987;25(7):883–914. doi:10.1016/0020-7225(87)90123-6.

[47] Tonti E. A direct discrete formulation of field laws: The cell method. CMES - Computer Modeling in Engineering and Sciences 2001;2(2):237–58.

[48] Ferretti E. The cell method: An enriched description of physics starting from the algebraic formulation. CMC-Comput Mater Con 2013;36(1):49–71.

[49] Tonti E. Why starting from differential equations for computational physics? Journal of Computational Physics 2014;257:1260–90. doi:10.1016/j.jcp.2013.08.016.

[50] Mooney M. A theory of large elastic deformation. Journal of Applied Physics 1940;11(9):582–92. doi:10.1063/1.1712836. arXiv:10.1063/1.1712836.

[51] Rivlin RS, Taylor GI. Large elastic deformations of isotropic materials. I. Fundamental concepts. Philosophical Transactions of the Royal Society of London Series A, Mathematical and Physical Sciences 1948;240(822):459–90. doi:10.1098/rsta.1948.0002.

[52] Blatz PJ, Ko WL. Application of Finite Elastic Theory to the Deformation of Rubbery Materials. Transactions of the Society of Rheology 1962;6(1):223–52. doi:10.1122/1.548937.

[53] Brockman RA. On the use of the blatz-ko constitutive model in nonlinear finite element analysis. Computers & Structures 1986;24(4):607–11. doi:10.1016/0045-7949(86)90199-9.

[54] Ciambella J, Saccomandi G. A continuum hyperelastic model for auxetic materials. Proceedings of the Royal Society A: Mathematical, Physical and Engineering Sciences 2014;470(2163):20130691. doi:10.1098/rspa.2013.0691.

[55] Crespo J, Montáns FJ. A continuum approach for the large strain finite element analysis of auxetic materials. International Journal of Mechanical Sciences 2018;135:441–57. doi:10.1016/j.ijmecsci.2017.11.038.

[56] Liu J, Zhang Y. Soft network materials with isotropic negative Poisson's ratios over large strains. Soft Matter 2018;14(5):693–703. doi:10.1039/c7sm02052j.

[57] Drozdov AD, deClaville Christiansen J. Modeling the elastic response of polymer foams at finite deformations. International Journal of Mechanical Sciences 2020;171:105398. doi:10.1016/j.ijmecsci.2019.105398.

[58] Misra A, Placidi L, dell'Isola F, Barchiesi E. Identification of a geometrically nonlinear micromorphic continuum via granular micromechanics. Zeitschrift fur Angewandte Mathematik und Physik 2021;72. doi:10.1007/s00033-021-01587-7.

[59] Zhu W, Blal N, Cunsolo S, Baillis D. Micromechanical modeling of effective elastic properties of open-cell foam. International Journal of Solids and Structures 2017;115-116:61–72. doi:10.1016/j.ijsolstr.2017.02.031.

[60] Carolan D, Mayall A, Dear J, Fergusson A. Micromechanical modelling of syntactic foam. Composites Part B: Engineering 2020;183:107701. doi:10.1016/j.compositesb.2019.107701.

[61] Choi JB, Lakes RS. Non-linear properties of polymer cellular materials with a negative Poisson's ratio. Journal of Materials Science 1992;27(17):4678–84. doi:10.1007/BF01166005.

[62] Maxwell JC. 1. on the equilibrium of elastic solids. Proceedings of the Royal Society of Edinburgh 1851;2:294–296. doi:10.1017/S0370164600036749.

[63] Zimmerman JA, WebbIII EB, Hoyt JJ, Jones RE, Klein PA, Bammann DJ. Calculation of stress in atomistic simulation. Modelling and Simulation in Materials Science and Engineering 2004;12(4):S319–32. doi:10.1088/0965-0393/12/4/s03.

[64] Eringen AC. Theory of Micropolar Elasticity. New York, NY: Springer New York. ISBN 978-1-4612-0555-5; 1999, p. 101–248. doi:10.1007/978-1-4612-0555-5_5.

[65] Duncan O, Allen T, Foster L, Senior T, Alderson A. Fabrication, characterisation and modelling of uniform and gradient auxetic foam sheets. Acta Materialia 2017;126:426–37. URL: https://www.sciencedirect.com/science/article/pii/S1359645417300046. doi:https://doi.org/10.1016/j.actamat.2017.01.004.

[66] Zhang QH, Su HD, Lin SZ, Shi GH. Algorithm for three-dimensional curved block cutting analysis in solid modeling. Computer Methods in Applied Mechanics and Engineering 2020;360(112721). doi:10.1016/j.cma.2019.112721.

[67] Bergstrom JS. Mechanics of solid polymers: theory and computational modeling. William Andrew; 2015.

[68] Sehlhorst HG, Jänicke R, Düster A, Rank E, Steeb H, Diebels S. Numerical investigations of foam-like materials by nested high-order finite element methods. Computational Mechanics 2009;45(1):45–59. doi:10.1007/s00466-009-0414-3.

[69] Ogden RW, Saccomandi G, Sgura I. Fitting hyperelastic models to experimental data. Computational Mechanics 2004;34(6):484–502. doi:10.1007/s00466-004-0593-y.

[70] Kenja K, Madireddy S, Vemaganti K. Calibration of hyperelastic constitutive models: the role of boundary conditions, search algorithms, and experimental variabil-

ity. Biomechanics and Modeling in Mechanobiology 2020;19(5):1935–52. doi:10.1007/s10237-020-01318-3.

[71] Crespo J, Duncan O, Alderson A, Montáns FJ. Auxetic orthotropic materials: Numerical determination of a phenomenological spline-based stored density energy and its implementation for finite element analysis. Computer Methods in Applied Mechanics and Engineering 2020;371:113300. doi:10.1016/j.cma.2020.113300.

[72] Bessa M, Bostanabad R, Liu Z, Hu A, Apley DW, Brinson C, et al. A framework for data-driven analysis of materials under uncertainty: Countering the curse of dimensionality. Computer Methods in Applied Mechanics and Engineering 2017;320:633–67. doi:10.1016/j.cma.2017.03.037.

[73] Staber B, Guilleminot J. Functional approximation and projection of stored energy functions in computational homogenization of hyperelastic materials: A probabilistic perspective. Computer Methods in Applied Mechanics and Engineering 2017;313:1–27. doi:10.1016/j.cma.2016.09.019.

[74] Huang GL, Sun CT. Band Gaps in a Multiresonator Acoustic Metamaterial. Journal of Vibration and Acoustics 2010;132(3). doi:10.1115/1.4000784.

[75] Wu Z, Liu W, Li F, Zhang C. Band-gap property of a novel elastic metamaterial beam with x-shaped local resonators. Mechanical Systems and Signal Processing 2019;134:106357. doi:10.1016/j.ymssp.2019.106357.

[76] Huang L, Chowdhury DR, Ramani S, Reiten MT, Luo SN, Azad AK, et al. Impact of resonator geometry and its coupling with ground plane on ultrathin metamaterial perfect absorbers. Applied Physics Letters 2012;101(10):101102. doi:10.1063/1.4749823. arXiv:10.1063/1.4749823.

[77] Ren X, Das R, Tran P, Ngo TD, Xie YM. Auxetic metamaterials and structures: a review. Smart Materials and Structures 2018;27(2):023001. doi:10.1088/1361-665X/aaa61c.

[78] Prakash D, Gupta N. Applications of metamaterial sensors: a review. International Journal of Microwave and Wireless Technologies 2022;14(1):19–33. doi:10.1017/S1759078721000039.

[79] Ma H, Wang K, Zhao H, Shi W, Xue J, Zhou Y, et al. Energy dissipation and shock isolation using novel metamaterials. International Journal of Mechanical Sciences 2022;228:107464. doi:10.1016/j.ijmecsci.2022.107464.

[80] Ma LH, Wang SD, Liu J, Gao H, Zhou W. The design and investigation of hydrogel-based metamaterials with ultra large negative hygroscopic expansion ratio. International Journal of Smart and Nano Materials 2022;13(1):114–29. doi:10.1080/19475411.2022.2049393. arXiv:10.1080/19475411.2022.2049393.

[81] Jenett B, Cameron C, T F. Discretely assembled mechanical metamaterials. Science Advances 2020;6(47):eabc9943. doi:10.1126/sciadv.abc9943. arXiv:https://www.science.org/doi/pdf/10.1126/sciadv.abc9943.